J Paleolimnol (2024) 71:101–124
https://doi.org/10.1007/s10933-023-00304-w

ORIGINAL PAPER

Quantifying conditions required for varve formation in meromictic Crawford Lake, Ontario, Canada: important process for delimiting the Anthropocene epoch

Brendan M. Llew-Williams · Francine M. G. McCarthy · Andrea M. Krueger · Nicholas L. Riddick · Michael D. MacKinnon · Krysten M. Lafond · R. Timothy Patterson · Nawaf A. Nasser · Martin J. Head · Michael F. J. Pisaric · Kevin W. Turner · Joseph I. Boyce · Uwe Brand

Received: 16 November 2022 / Accepted: 3 October 2023 / Published online: 3 November 2023
© The Author(s), under exclusive licence to Springer Nature B.V. 2023

Abstract Varved sediments in meromictic Crawford Lake consist of dark–light couplets of organic matter (primarily phytoplankton and amorphous organic matter) capped by calcite crystals. The crystals precipitate in the alkaline epilimnion between spring and fall turnover, consistent with Langelier Saturation Index calculations that predict calcite precipitation when pH and temperature exceed 7.76 and ~ 15 °C, respectively. Climate, primary production, and the pH of the epilimnion control lamina thickness: acid rain primarily affects the precipitation and accumulation of calcite crystals, whereas both endogenic calcite and authigenic organic matter are affected by climate and primary production. Thin varves, often with barely perceptible light-coloured calcite laminae were deposited between the late 1940s and mid-1970s, when the pH of the epilimnion fell slightly in response to deterioration in air and water quality associated with rapid industrialization. Conditions required for precipitation of calcite laminae were absent during the sixteenth to mid-nineteenth centuries, an interval corresponding to the Little Ice Age when no human impact affected the catchment. Varves dating from 1867 CE onwards (the Canadian Zone) facilitate the candidacy of the deep basin sediments of Crawford Lake to define the Anthropocene epoch.

Keywords GSSP · Calcite · Climate · Eutrophication · Varve chronology

Introduction

Lacustrine sedimentary laminations are classified as clastic, biogenic, or endogenic, and often accumulate as a mixture of these end members in environments

Supplementary Information The online version contains supplementary material available at https://doi.org/10.1007/s10933-023-00304-w.

B. M. Llew-Williams · F. M. G. McCarthy (✉) · N. L. Riddick · M. J. Head · U. Brand
Department of Earth Sciences, Brock University, St. Catharines, ON L2S 3A1, Canada
e-mail: fmccarthy@brocku.ca

A. M. Krueger
Department of Biological Sciences, Brock University, St. Catharines, ON, Canada

M. D. MacKinnon
OSPM Solutions, Hamilton, ON, Canada

K. M. Lafond · R. T. Patterson · N. A. Nasser
Ottawa-Carleton Geoscience Center and Department of Earth Sciences, Carleton University, Ottawa, ON, Canada

M. F. J. Pisaric · K. W. Turner
Department of Geography and Tourism Studies, Brock University, St. Catharines, ON, Canada

J. I. Boyce
School of Earth, Environment and Society, McMaster University, Hamilton, ON, Canada

associated with seasonal climate variability (Anderson and Dean 1988; Zolitschka et al. 2015). The cyclical deposition of varves is primarily controlled by annual climatic variation and watershed conditions, including geology, hydrology, vegetation coverage, and local anthropogenic impact, which can affect the potential for sediments to accumulate and be preserved as alternating laminae (Zolitschka et al. 2015). Direct and incremental dating of laminations (i.e., 'varve-counting') provides the opportunity to achieve annual resolution (Ekdahl et al. 2004; Lafond et al. 2023; McCarthy et al. 2023) (Fig. S1). This allows changes recorded by various biological and physicochemical proxies in the sediments to be correlated to calendar ages and events in the historic record, including increased anthropogenic activity (Ekdahl et al. 2007; Randsalu-Wendrup et al. 2014; Krueger and McCarthy 2016; Gushulak et al. 2022).

Endogenic laminations consist of chemically precipitated sediments that can be either physically or biologically induced (Last 2001). The precipitation of minerals, including calcite ($CaCO_3$), occurs during periods of elevated temperatures, when algal blooms decrease acidity in the epilimnion through carbon fixation, lowering calcite solubility. Biogenic laminations form in temperate, nutrient-rich lakes, when the biomass of primary producers and their consumers descend to the lakebed as organic detritus, with the largest influx of total organic carbon (TOC) occurring when epilimnion temperatures drop (Zolitschka et al. 2015).

Crawford Lake

Crawford Lake is a small (~ 2.4 hectare) lake that occupies a deep (~24 m) sinkhole dissolved in dolomitic limestones of the Silurian Lockport Group (Fig. 1). The lake is permanently stratified due to its depth, high depth-to-surface-area ratio, hydrology, and recharge characteristics (Dickman 1979, 1985; Llew-Williams 2022). The lake has a well-developed chemocline at ~15.5 m depth with no active mixing between the monimolimnion and superjacent mixolimnion (Rybak and Dickman 1988; Heyde 2021; Llew-Williams 2022).

In contrast to most meromictic lakes, concentrations of dissolved oxygen in the monimolimnion of Crawford Lake are well above the hypoxic limit (Heyde 2021). This unusual limnology has been attributed to inputs of well-oxygenated groundwater from bedrock aquifers, recharged ~1 km away (Llew-Williams 2022; McCarthy et al. 2023). The inflow of groundwater from karstic Silurian limestones (Brunton 2009; Priebe et al. 2018) dominates the water properties of the monimolimnion. The Gasport Formation crops out in the lower part of the Crawford Lake basin, inferred from the dip of stratigraphic units reported by Armstrong and Carter (2010). High electrical conductivity and ionic composition measured below the chemocline closely resemble the chemical signature of local groundwaters reported in the Ontario Provincial Groundwater Monitoring Network (Llew-Williams 2022). The highest electrical conductivity, found in the lower part of the monimolimnion, may represent baseflow through the Lockport Group (Fig. 1), particularly along the contact between the Gasport and Goat Island formations where hydraulic conductivity is highest (Priebe et al. 2018; Priebe 2019). The Goat Island Formation, which crops out as steep shoreline cliffs along the north shore of Crawford Lake, has a mean hydraulic conductivity of 7×10^{-6} m s^{-1}, and the underlying Gasport Formation has an even higher hydraulic conductivity of 5×10^{-5} m s^{-1} (Priebe et al. 2018).

Meromixis appears to predate the inflow of well-oxygenated groundwater to the monimolimnion; the fossil pigment okenone produced by obligately anaerobic sulfur-reducing purple bacteria is absent from sediments deposited since the early sixteenth century, although anoxia prevailed through the interval of Indigenous agriculture spanning the late thirteenth through fifteenth centuries (Heyde 2021; McCarthy et al. 2023; P. Leavitt unpublished data). Despite the abundant supply of oxygen below the chemocline, high concentrations of ions appear to have prevented the colonization of what is essentially a groundwater window by benthic invertebrates larger than stygofaunal ostracods (Heyde 2021). Well-defined varve couplets of alternating calcite and organic matter that accumulated below the chemocline during the Indigenous and colonial–Canadian impact intervals (since the early nineteenth century) remain undisturbed, providing annual resolution.

The varved record of Crawford Lake is one of the sedimentary successions studied as a potential Global boundary Stratotype Section and Point (GSSP) following agreement within the AWG that the base of the Anthropocene should align with stratigraphic

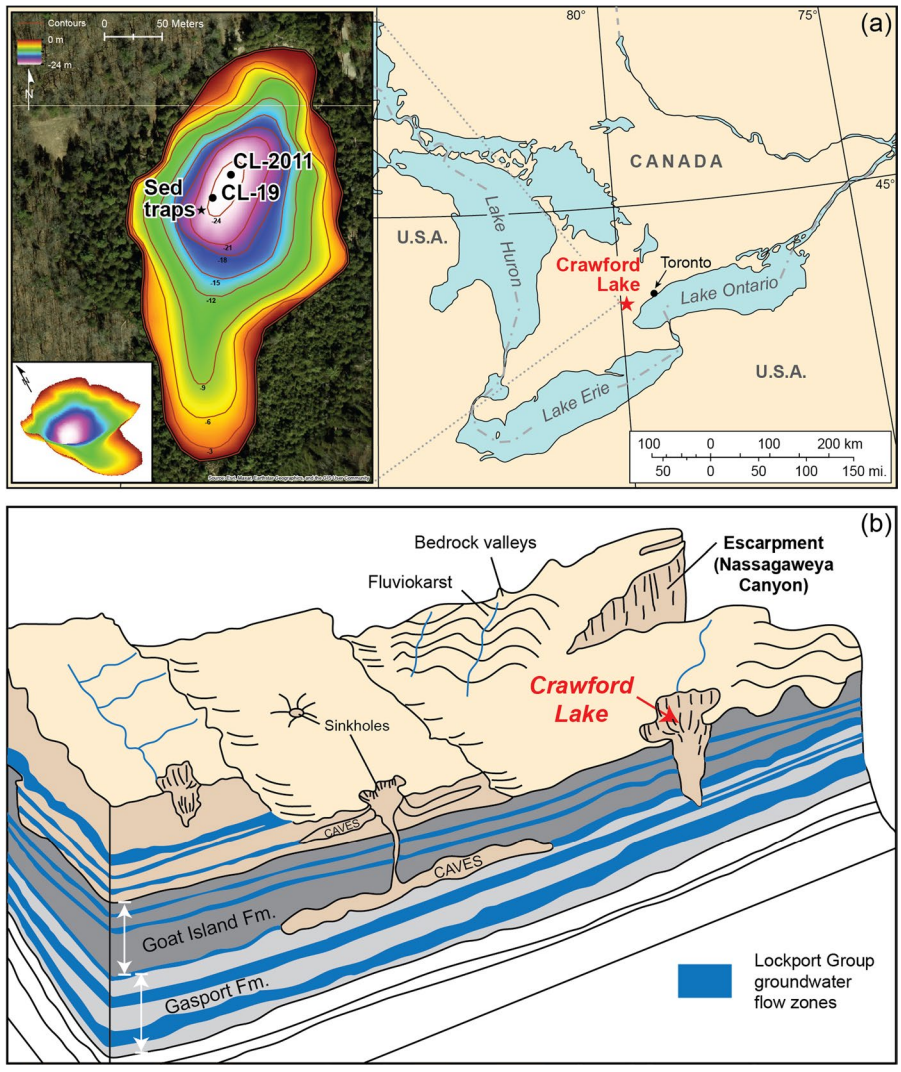

Fig. 1 **a** Location of Crawford Lake in southern Ontario and generalized bathymetry map (contour interval = 3 m) showing locations of sediment traps and freeze core CL-2011 and gravity core CL-19 in the deep basin of this meromictic lake (inset generated using ArcGIS). The lake occupies a >22 m deep, karst sinkhole in the Silurian (Lockport Group) dolomitic limestones, about 1 km from Nassagaweya Canyon. **b** Schematic block diagram showing karst features and groundwater flow zones in bedrock aquifers of the Goat Island and Gasport formations (Brunton 2009) that are inferred to transect the Crawford Lake basin based on regional dip of strata published by Armstrong and Carter (2010)

signals dating to the mid-twentieth century (Waters et al. 2023) to reflect a fundamental shift in the Earth System known as the 'Great Acceleration' (Steffen et al. 2015, 2016; Head et al. 2022). The varve chronology of Lafond et al. (2023) based on ultra-high-resolution imagery (Fig. 2) is consistent with the $^{239+240}$Pu record of nuclear fallout in this and several other cores from the deep basin of Crawford Lake (Fig. 3), where several proxies record the 'Great Acceleration' of the mid-twentieth century. These by-products of nuclear weapons testing provide a key marker for the proposed Anthropocene epoch whose base would be defined in a lamina corresponding to a single calendar year (Zalasiewicz et al. 2019; Waters et al. 2023).

The varved sediments that accumulate below the chemocline of Crawford Lake were determined to result from a combination of endogenic calcite precipitation during the summer and biogenic accumulation of organic matter, most rapidly during fall turnover (Dickman 1979, 1985). The light laminae at Crawford Lake allow the development of varve chronology, providing (sub-)annual precision for the dark–light couplets of organic matter capped by calcite crystals. This has been confirmed by varve counts in freeze cores collected and analysed since the early 1970s. Ekdahl et al. (2004) obtained 28 Accelerator Mass Spectrometry (AMS) radiocarbon ages from upland-plant macrofossils in the upper 80 cm of a freeze core collected in 2001, spanning the last

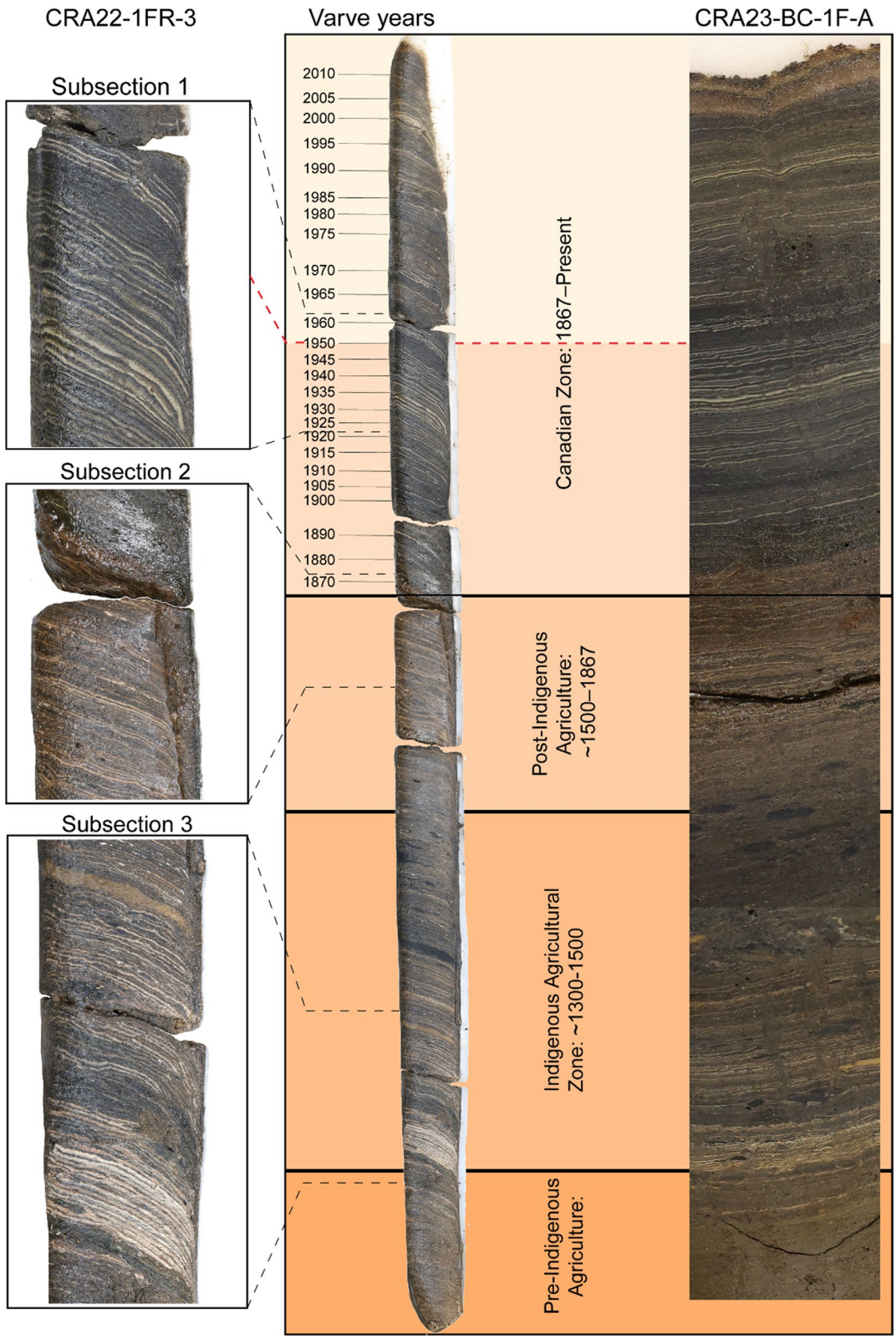
CRA22-1FR-3
Varve years
CRA23-BC-1F-A
Subsection 1
Subsection 2
Subsection 3
2010
2005
2000
1995
1990
1985
1980
1975
1970
1965
1960
1950
1945
1940
1935
1930
1925
1920
1915
1910
1905
1900
1890
1880
1870
Canadian Zone: 1867–Present
Post-Indigenous Agriculture: ~1500–1867
Indigenous Agricultural Zone: ~1300-1500
Pre-Indigenous Agriculture:

◂**Fig. 2** Composite image (side-view) of sections along the length of core CRA22-1FR-3, archived in the National Biodiversity Cryobank of Canada and of the face of one of the freeze cores recovered in April 2023 (core CRA23-BC-1F-A, being analysed for ^{239}Pu at annual resolution) illustrating how easy it is to correlate the distinctive varved sediment across the deep basin of Crawford Lake. A thin calcite lamina capping the 1950 varve, near the base of a dark layer that can be traced across the basin, has been proposed as a GSSP (McCarthy et al. 2023), and the lighter shading illustrates the proposed Anthropocene epoch enlarged in subsection 1. Subsection 2 shows the transition from reddish brown to dark brown organic matter in the mid-nineteenth century, when logging began in the catchment. The lower enlargement (subsection 3) illustrates the most prominent calcite laminae, deposited when an agricultural settlement was established during the Medieval Warm Period. Calcite laminae are sporadic in sediments predating cultural eutrophication. Modified from Lafond et al. (2023)

1100 years, confirming that the *Ambrosia* pollen-rich couplets through the Canadian Zone (since 1867 CE) are varves (Boyko 1973; Boyko-Diakonow 1979).

This study

Improved understanding of varve formation in this unusual meromictic lake with a rich prehistoric cultural record is important, particularly given its potential role in defining the base of the Anthropocene (Fig. 2). Refining our understanding of the conditions required for calcite crystals to form and accumulate on the lakebed should help explain the breakdown in varve deposition between the Indigenous and colonial–Canadian impact intervals. This is crucial to support the contention that the 'summer' calcite laminae are likely to accumulate for the foreseeable future in the deep basin, and thus provide annual resolution for the ongoing proposed Anthropocene epoch (McCarthy et al. 2023).

Materials and methods

Physical and chemical monitoring

Physical and chemical data were collected during 12 surveys spanning all seasons between August 2018 and September 2021 (Llew-Williams 2022). Depth profiles of temperature (°C), pH, and electrical conductivity (µS cm^{-1}) were collected from Crawford Lake using a Horiba U-5000 multiprobe at 1-m intervals in August of 2018, February, September and October of 2019, February, June, July, August and September of 2020, and September of 2021, with a higher sampling resolution (every 0.25 m) between 14 and 18 m in June 2021. During an October 2020 survey, measurements were collected only for depths of 0, 5, 12, and 18 m. The multiprobe was calibrated prior to each survey using the Horiba U-50 series built-in 'auto-calibration' feature using a standard pH 4 solution (Horiba 2009). Water samples were collected with a Kemmerer bottle. They were transferred unfiltered on site into high-density polyethylene (HPDE) pre-cleaned and site-rinsed bottles, and delivered to E3 Laboratories, Niagara-on-the-Lake, for chemical analysis. Alkalinity and bicarbonate measurements were made by titration (APHA 2320B) of filtered samples. Calcium, magnesium, and potassium were measured using ICP-AES (EPA 6010c). Measurements of nitrate, nitrite, total nitrogen, reactive phosphorus, and total phosphorus employed APHA 4500. pH was measured using method APHA 4500 H-B and standard HACH tests were conducted for chloride, fluoride, sodium, and chemical oxygen demand (COD). Full details about sampling and analysis are available in Llew-Williams (2022).

Langelier saturation index calculations

The Langelier Saturation Index (LSI) is a calculated water property for predicting whether calcium carbonate dissolution or precipitation is likely (Langelier 1936, 1946). Potential calcite ($CaCO_3$) precipitation or dissolution in water is a function of pH, temperature, hardness, alkalinity, and electrical conductivity (a proxy of total dissolved solids, TDS). With this index, the saturation point pH (pH_s) of calcium carbonate can be estimated. LSI is the difference between monitored pH, and calculated saturation pH_s as shown in Eq. (1). An online calculator (Lenntech 2021; Hach Method 8073 2021) was applied to water properties observed between February 2019 and June 2021. With this tool, pH_s was calculated by depth and season to identify zones of likely calcite precipitation.

$$LSI = pH - pH_s \quad (1)$$

When pH_s is equal to pH the solution is balanced, when $pH_s < pH$ precipitation could occur, and when $pH_s > pH$ dissolution could occur.

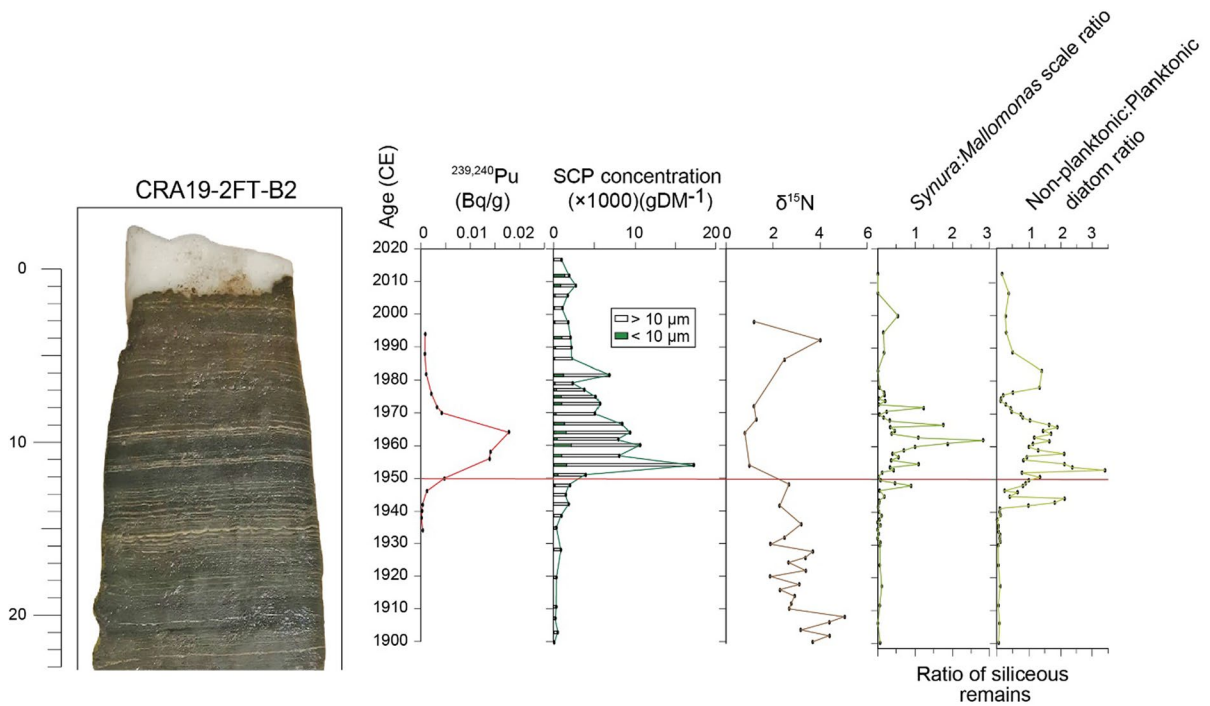

Fig. 3 Photograph of core CRA19-2FT-1FRA and plot of key markers of the Great Acceleration: abundant spheroidal carbonaceous particles (SCPs) and depleted values of $\delta^{15}N$, coinciding with rapid increase in nuclear fallout ($^{239+240}Pu$) from thermonuclear weapons testing. The lowermost of two dark bands separated by a triplet of prominent calcite laminae deposited in the summers of 1956, 1957 and 1958, is attributed to acidification associated with fossil fuel emissions, notably from steel mills in nearby Hamilton. This is supported by siliceous microfossil data indicative of increased light penetration (increase in the deep-dwelling colonial chrysophyte *Synura* spp. and non-planktonic diatoms) (Marshall et al. 2023). Modified from McCarthy et al. (2023)

Saturation index calculations

The Saturation Index (SI) is another calculated water property used for predicting whether dissolution or precipitation of a mineral (including $CaCO_3$) is likely to occur under various hydrological conditions. Similar to the LSI, which is used specifically to predict the saturation point of calcium carbonate, SI calculations utilize pH, and factors of temperature, calcium concentration, and alkalinity to predict if precipitation is likely to occur in the water column. By utilizing Eq. (2) and the water properties observed in Crawford Lake between February 2019 and June 2021, SI was calculated and compared to the results of the LSI calculations to confirm and identify zones of probable calcite precipitation both seasonally and spatially. The factors for temperature, calcium concentrations, and alkalinity used in Eq. (2) are displayed in Table S4.

$$SI = pH + Temperature\ Factor + Calcium\ Factor + Alkalinity\ Factor - 12.1 \quad (2)$$

When $SI = 0$ the solution is balanced, when $SI > 0$ precipitation could occur, and when $SI < 0$ dissolution could occur.

Sediment-trap analysis

A line with two sediment traps was deployed on August 20, 2020, with the upper trap at 5.5 m and the lower trap at 15.5 m (Fig. 4a). The contents of the traps were sampled from a Zodiac inflatable boat on October 19, 2020 (capturing summer processes), and June 18 and September 17, 2021 (capturing fall, winter, and spring; and summer processes respectively). Samples were fixed

with Lugol's iodine solution in the field and processed for analysis at Brock University. To analyse the inorganic fraction, sediment-trap samples were treated with 30% hydrogen peroxide (H_2O_2) in a hot water bath for 15–20 min to oxidize most of the organic matter, but microscope smear slides were made before and after treatment to assess the full content of the traps. The organic fraction of the sediment-trap samples was analysed after standard palynological treatment, but omitting the use of harsh oxidants (e.g., acetolysis treatment) that selectively destroy susceptible organic-walled microfossils (Riddick et al. 2017). For palynological analysis, a tablet containing a known quantity of *Lycopodium clavatum* spores (Batch #414831, 12,100 ± 1892 spores/tablet, Lund) was added to samples of 2.5 mL volume during treatment with warm (not boiling) weak (7%) HCl to dissolve carbonates (predominantly precipitated calcite crystals, and rare ostracod valves). This was followed by HF treatment to dissolve silicates, these being predominantly siliceous microfossils (Gushulak et al. 2022) but also rare detrital silicate grains that are particularly common in sediments with other indicators of terrigenous influx. The acid-resistant residue after washing but without sieving was then mounted on glass-microscope slides using glycerine jelly. Slides were analyzed qualitatively for sediment-trap constituents including palynomorphs using a Leica DM750 microscope at 400× magnification (Heyde 2021). For palynological sediment-trap analysis, sediments were processed as above but the residue was sieved using 15 µm Nitex© mesh prior to mounting on slides using glycerine jelly. Organic-walled remains of algae and their consumers were identified to the highest possible taxonomic resolution using a variety of sources, most of which are cited in McCarthy et al. (2021).

Sediment-core analysis

On January 25, 2011, a coring expedition used a frigid fingernail sampler, a narrow hollow aluminum wedge filled with an ethanol and dry ice slurry to penetrate the lakebed (~22.5 m water depth), freezing sediments onto the ultra-cold aluminum face of the sampler. The core faces were removed from the sampler using warm water, wrapped in plastic film, and one face of core CL-2011 was transported to Brock University where it was kept in a freezer. It was previously subsampled for palynological analysis (Krueger and McCarthy 2016; McCarthy et al. 2018; Heyde 2021) and for radiocarbon analysis to identify the bomb pulse (McCarthy et al. 2023), but when accessed for this study in late summer 2021, the core had thawed and slumped slightly. Fortunately, since it had been stored flat on a plywood base, the thawed core face retained sufficient integrity to allow characteristic marker varves (Fig. 2) to be identified. The light and dark laminae from the thickest varve (dated to 1935 CE; McCarthy et al. 2023) were sampled separately using a small spatula and smear slides were made from each, using melted glycerine jelly as a mounting medium. Slides were analyzed qualitatively using a Leica DM750 microscope at 400× magnification and photographed using a Leica MC120HD digital imaging camera (Lafond et al. 2023).

Gravity core (CL-19; Fig. 1a) was collected from 22.1 m water depth using UWITEC sampler on February 19, 2019. The core was immediately moved to the core extruder and water above the sediment–water interface was removed to avoid loss of sediment through degassing. The core was extruded in the field at 1-cm intervals into Whirl–pak© bags and transported to the Water and Environment Laboratory at Brock University, where they were kept in cold storage (4 °C). This core was processed and analysed for several proxies as part of the investigation into the potential of the varved succession of Crawford Lake to define the Anthropocene formally (McCarthy et al. 2023).

Micro-X-ray fluorescence (µ-XRF) geochemical analysis was performed on cores CL-2011 and CL-19 using an ITRAX core scanner (McMaster University) with a Cr tube. The upper 20 cm of the thawed face of core CL-2011 (spanning most of the Canadian Zone, since 1867 CE) was analyzed at a 200-µm sample intervals with a 15 second analysis time and constant power settings (30 kV, 25 mA). Representative 1-cm subsamples from core CL-19 were analysed in a sequential sample tray using the same settings (Gregory et al. 2017). XRF data were batch analyzed using QSpec™ software (Cox Analytical Systems), and element profiles normalized using the ratio of coherent to incoherent scatter (CIR) to minimize matrix effects caused by variations in sediment porosity, moisture, and organic content (Gregory et al. 2017). From the available elements, calcium (Ca) was selected as an

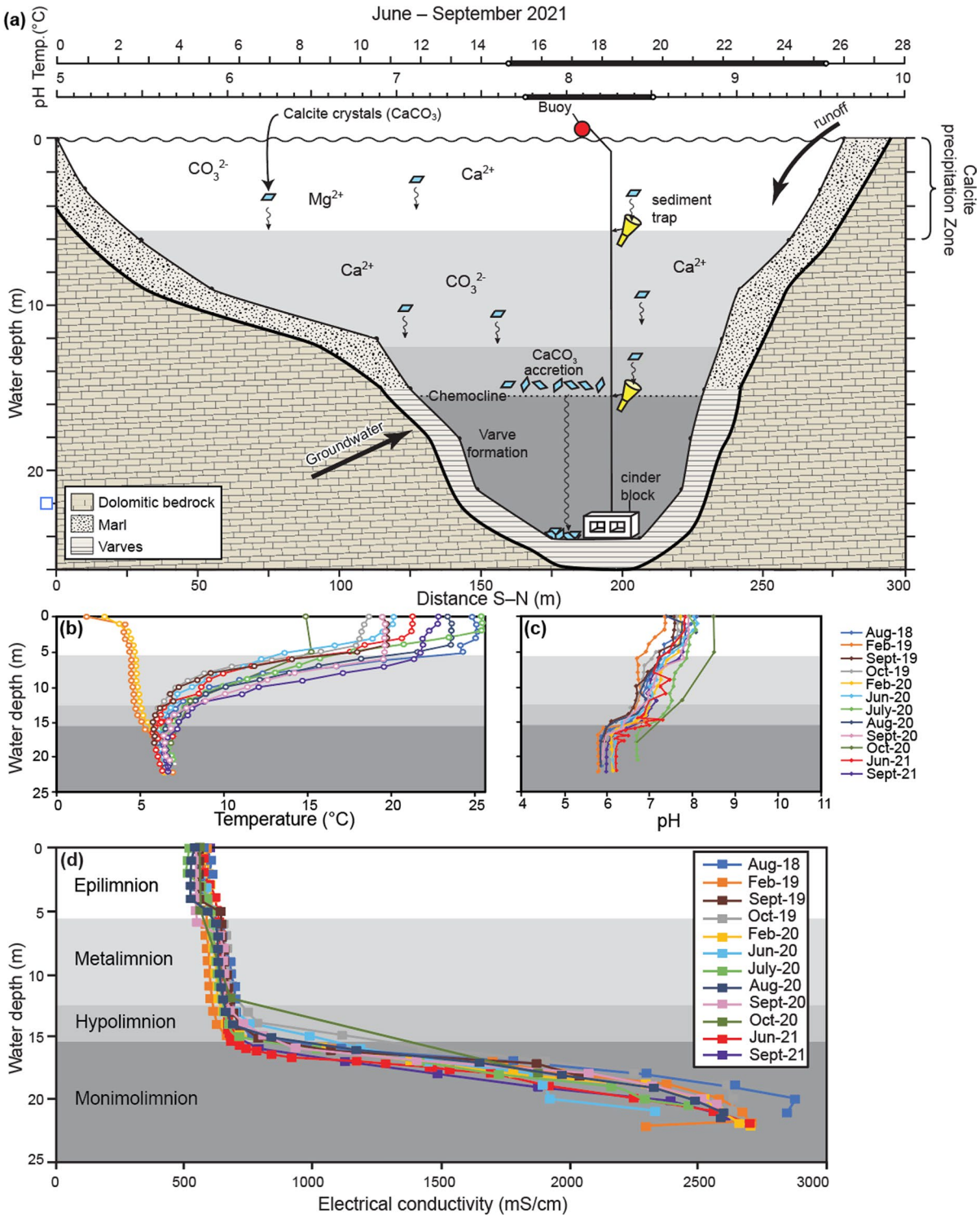
(a)
June – September 2021
pH Temp.(°C)
Calcite crystals ($CaCO_3$)
Buoy
runoff
CO_3^{2-}
Mg^{2+}
Ca^{2+}
sediment trap
Calcite precipitation Zone
Water depth (m)
$CaCO_3$ accretion
Chemocline
Varve formation
Groundwater
cinder block
Dolomitic bedrock
Marl
Varves
Distance S–N (m)
(b)
Temperature (°C)
(c)
pH
(d)
Epilimnion
Metalimnion
Hypolimnion
Monimolimnion
Electrical conductivity (mS/cm)
Aug-18
Feb-19
Sept-19
Oct-19
Feb-20
Jun-20
July-20
Aug-20
Sept-20
Oct-20
Jun-21
Sept-21

◂**Fig. 4** **a** Range of temperature and pH values that promote the precipitation of endogenic calcite and accumulation on the lakebed of Crawford Lake during the summer, and characteristics that isolate the monimolimnion (darkest shading) derived from the multiyear dataset of (**b**) temperature, (**c**) pH, and (**d**) electrical conductivity. Sediment traps at the boundary between the epilimnion (unshaded) and metalimnion (lightest grey shading) and along the chemocline between the hypolimnion (medium shading) and monimolimnion confirm the seasonal and spatial pattern of calcite sedimentation predicted by Langelier Saturation Index calculations: the minimum 15 °C and pH 7.8 were measured only in the upper 6 m of the water column during summer and early fall. The density contrast along the chemocline appears to slow the sinking of calcite crystals precipitated in the epilimnion to uppermost metalimnion, allowing the abundant Ca^{+2}, CO_3^{-2} and HCO_3^{-} ions in the monimolimnion to accrete onto these nuclei (Fig. 6) as suggested by Morse et al. (2007) and Müller et al. (2016)

indicator of authigenic $CaCO_3$ production, and titanium (Ti) and potassium (K) as indicators of terrigenous sediment inputs (Rothwell and Croudace 2015). Lead (Pb) and copper (Cu) were selected as indicators of anthropogenic metal contaminants associated with twentieth century activities.

Samples from core CL-19 spanning the last millennium were also analysed for pollen and non-pollen palynomorphs (McCarthy et al. 2023), with chronological control provided by seven additional AMS radiocarbon ages of upland-plant macrofossils in addition to the well-dated pollen stratigraphy. For this study, the transfer functions of Bartlein and Whitlock (1993) for the closest calibration region (45–55° N, 75–87° W) were applied to the pollen data to reconstruct mean July and January temperatures. Previously unpublished results and measurements referred to in this study are given in the Supplemental Materials, and additional details on methods can be found in Llew-Williams (2022).

Results

Physical and chemical characteristics, water column

Seasonal variations in water temperature were most prominent in the epilimnion (0–5.5 m; 1.8–25.4 °C), followed by the metalimnion (5.5–12.5 m; 4.5–19.5 °C) (Fig. 4b, Table 1). Relatively constant year-round temperatures were found below a seasonal thermocline, ranging from 4.7 to 8.0 °C in the hypolimnion (12.5–15.5 m) and 5.3 to 7.2 °C in the monimolimnion (15.5–24.0 m). Water pH decreased with depth, from an average of ~ 7.7 in the epilimnion to ~ 7.1, ~ 6.8, and ~ 6.1 in the metalimnion, hypolimnion, and monimolimnion, respectively (Fig. 4c, Table 1). Relatively small changes in salinity were measured throughout an annual cycle (Fig. 4d) but electrical conductivity was 4 to 5 times higher in the monimolimnion (~ 1900 µS cm^{-1}) than in the epilimnion (~ 570 µS cm^{-1}). The highest electrical conductivity was measured in the lower 5 m of the water column, where the mean was close to 2500 µS cm^{-1}. The resulting density contrast produces a strong, stable pycnocline, further enhancing meromixis. Calcium concentrations and alkalinity remained stable throughout the mixolimnion (0–15.5 m) but increased sharply across the chemocline (Table 1, Fig. S2). Calcium concentrations increased from ~ 70 to 150 mg L^{-1} within the monimolimnion, and alkalinity increased from ~ 300 to 850 mg L^{-1} (expressed as $CaCO_3$) (Supplemental Table 1).

LSI and SI calculations

Between June and October of 2020, water temperatures in the epilimnion (0–5.5 m) ranged from 15 to 25 °C, and water chemistry supported calcite precipitation: alkalinity of 240 to 290 mg L^{-1}, calcium content of 50–65 mg L^{-1}, electrical conductivity of 510–620 µS cm^{-1}, and pH greater than 7.8 (Fig. 4, Table 2). At no point between fall and spring turnover did measurements yield positive LSI values (Fig. 5, Table 2).

Sediment-trap samples

Distinct differences in the abundance and size of calcite crystals were identified in smear slides of sediment-trap samples, both seasonally and through the water column (Fig. 6). Many small (~ 2–10 µm) calcite crystals precipitated in the epilimnion accumulated in the upper trap, particularly during the summer of 2021. Between fall and spring turnover, the inorganic fraction in both the upper and lower traps was dominated by biogenic silica and contained a few relatively large conchoidally fractured grains of detrital quartz. Together with amorphous organic matter representing decomposition by bacteria, the remains of organic-walled plankton were abundant in the upper trap during both mid-August to mid-October

Table 1 Summary of the physical and chemical variables required for LSI and SI analysis sampled from Crawford Lake including the averaged sampling value (bold), the maximum sampling range, and number of samples (n); note: alkalinity expressed as $CaCO_3$

	Temperature (°C) (mean/range)	pH (mean/range)	Conductivity (µS cm^{-1}) (mean/range)	Ca^{2+} (mg L^{-1}) (mean/range)	Alkalinity (mg L^{-1}) (mean/range)
Epilimnion 0–5.5 m	***17.0***/1.8–25.4 (n = 62)	***7.7***/6.9–8.5 (n = 62)	***567***/514–641 (n = 62)	***55.7***/48.4–66.2 (n = 17)	***255***/226–290 (n = 17)
Metalimnion 5.5–12.5 m	***9.8***/4.5–19.5 (n = 71)	***7.1***/6.7–7.9 (n = 71)	***638***/543–697 (n = 71)	***66.1***/49.4–79.1 (n = 15)	***288***/251–312 (n = 15)
Hypolimnion 12.5–15.5 m	***6.4***/4.7–8.0 (n = 30)	***6.8***/6.1–7.5 (n = 30)	***715***/612–1110 (n = 30)	***72.2***/65.9–84.6 (n = 10)	***306***/296–327 (n = 10)
Monimolimnion 15.5–23 m	***6.3***/5.3–7.2 (n = 72)	***6.1***/5.8–6.8 (n = 72)	***1892***/741–2700 (n = 72)	***146***/79–215 (n = 20)	***848***/326–1410 (n = 20)

Table 2 Months and depths in the water column of Crawford Lake where calcite precipitation is predicted by positive LSI values (a function of pH, water temperature, and concentrations of calcium, alkalinity, and electrical conductivity; complete data in Table S3) and confirmed with positive SI values (a function of pH, water temperature, and concentrations of calcium and alkalinity; complete data in Table S1)

Date	Depth (m)	Temp. (°C)	pH	E. Cond. (µS cm^{-1})	Ca^{2+} (mg L^{-1})	Alkalinity (as mg L^{-1} $CaCO_3$)	pH_s	LSI ($pH - pH_s$)	SI
24-Jun-2020	0	20.2	8.02	545	54.4	244	7.8	0.22	0.18
23-Jul-2020	0	25.4	7.93	521	48.4	240	7.7	0.23	0.07
	2	25.4	8.09	514	48.5	241	7.7	0.39	0.26
	4	20.8	7.94	591	61.9	274	7.6	0.34	0.22
	6	15.8	7.88	615	65.1	290	7.7	0.18	0.09
20-Aug-2020	**2**	**23.6**	**7.76**	**522**	**50.7**	**248**	**7.7**	**0.06**	**-0.04**
28-Sep-2020	**2**	**19.6**	**7.91**	**539**	**49.8**	**254**	**7.8**	**0.11**	**0.02**
	6	**19.5**	**7.81**	**543**	**49.4**	**251**	**7.8**	**0.01**	**-0.09**
19-Oct-2020	0	14.9	8.50	558	54.4	263	7.8	0.70	0.53
	4	15.2	8.51	559	51.8	246	7.9	0.61	0.51

Bold identifies months when calcite is not precipitated in the surface waters, but instead slightly deeper where photoinhibition disrupts primary production less and freshwater runoff is less likely to lower pH. SI values indicate similar findings to the LSI calculations, with the exception of negative values in the epilimnion in August and September 2020. Complete dataset available in Llew-Williams (2022)

2020 ('October') and mid-June to mid-September 2021 ('September') intervals, with an influx of ~ 1865 and 1100 organic-walled plankton per day through the epilimnion (Fig. 7, Table 3). The remains of dinoflagellates and green algae dominated the assemblages, whereas zooplankton (cladocerans and the rotifer genus *Keratella*) made up only 3.4% of the assemblage in summer and 12.6% in fall. Much lower influx was recorded over the longer interval between October 2020 and June 2021, with an influx of ~ 240 plankton per day through the epilimnion. This phytoplankton assemblage was least diverse, and strongly dominated by thecae of the dinoflagellate *Peridinium volzii* and conjugated cells of the desmid *Cosmarium benum.*

By far the highest concentration of organic-walled plankton was sampled from the lower trap in the fall, with an influx of ~ 12,650 individuals per day between mid-August and mid-October 2020. These were primarily cellulosic thecae of *Peridinium volzii, Peridinium willei*, and *Peridiniopsis* sp., and dinosporin cysts of *Parvodinium inconspicuum*, with zooplankton making up 4.2% of the assemblage. Unlike the upper trap, the lowest influx of organic-walled plankton to the chemocline occurred in the summer rather than in winter, with an influx of only 390 individuals per day in June–September 2021 (most of which were

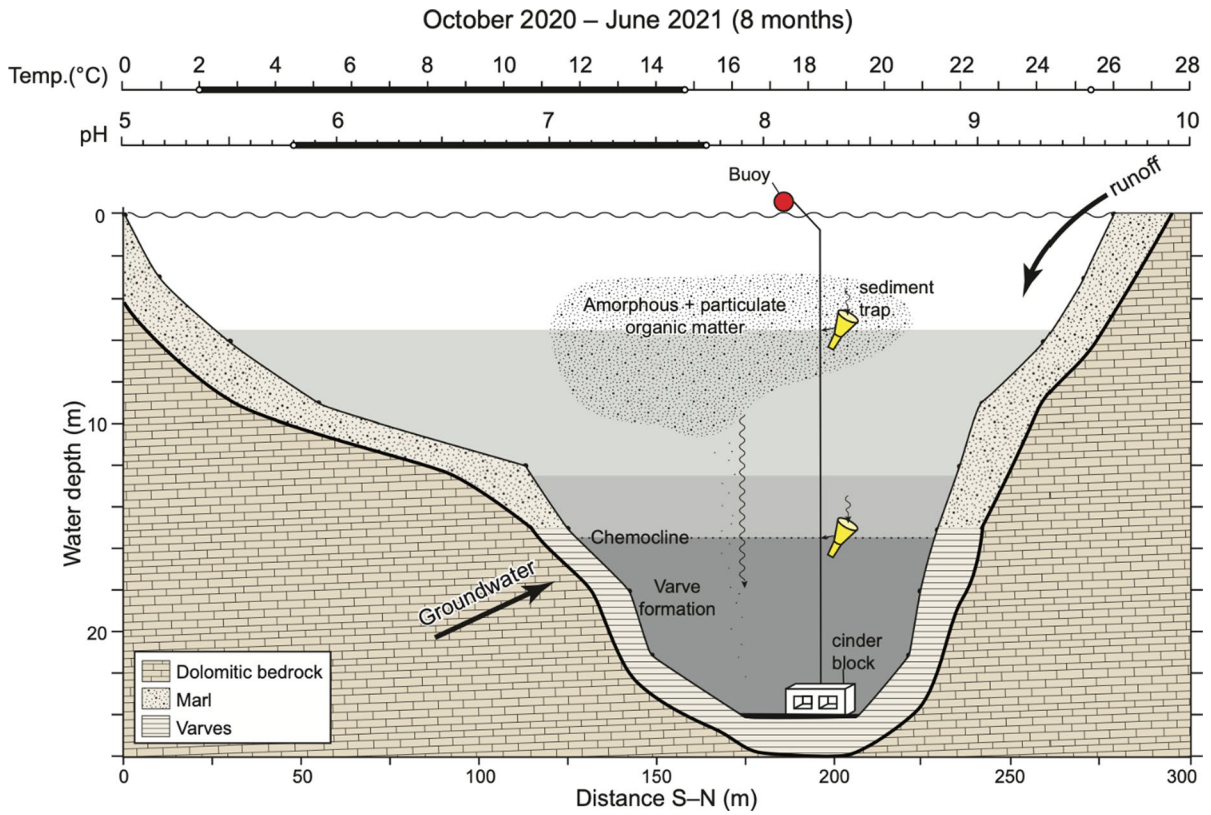

Fig. 5 Range of temperature and pH measured between fall and spring turnover through the water column of Crawford Lake. These did not yield positive LSI values (contrast Fig. 4). The most rapid influx of organic matter through the epilimnion (upper trap) and to the monimolimnion (lower trap) occurred in the fall, when temperatures cooled, and incident solar radiation declined in the upper part of the mixolimnion. The range of temperature and pH measured between fall and spring turnover does not satisfy the LSI requirements for precipitation of calcite anywhere in the water column. This confirms the assumption that dark laminae represent fall–winter accumulation and that light-coloured calcite caps the organic matter in the summer

cysts of *P. inconspicuum*) compared to 646 plankton per day between mid-August and mid-October. The highest relative abundance of zooplankton (29.6%) was observed in the lower trap collected in June 2021, representing accumulation since mid-October 2020.

Freeze-core sedimentology and geochemistry

Microscopic examination of smear slides made from the light and dark laminae from the thick 1935 couplet (Fig. S3) in core CL-2011 confirms that crystals of calcite are the dominant component of the white lamina. Little organic matter was present, and few microfossils were observed. The dark lamina comprised amorphous and particulate organic matter, including palynomorphs such as the rotifer lorica in Fig. S3. Minute (<5 μm) crystals of calcite were present in the dark lamina, but in much lower abundance than in the white lamina.

μ-XRF analysis revealed variations in elemental composition that are not discernible at the light–dark lamina scale, but rather over longer intervals that correspond to the centimeter-scale bands of darker and lighter coloured sediment that comprise multiple varves, such as the prominent calcite laminae deposited in the summers of 1956, 1957 and 1958, and through the warm, dry 'Dust Bowl' of the 1930s (Figs. 8a, S1). For the entire core, Ca was inversely correlated with Fe ($r = -0.22$) and showed no significant correlation with other terrigenous-derived elements (Fig. 8b). In the period following 1950 (8–13 cm core interval; Fig. 8c), Ca was also inversely

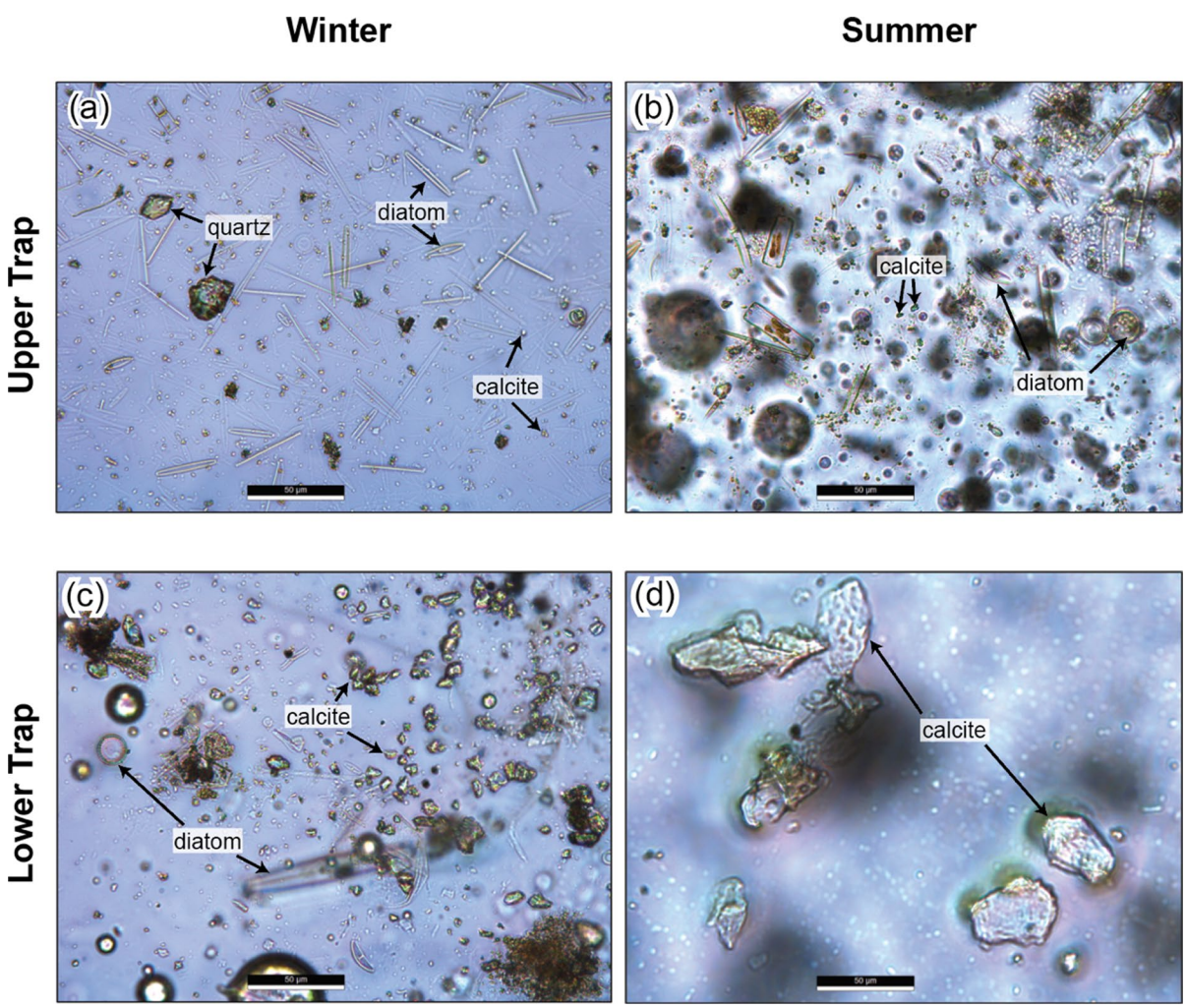

Fig. 6 Representative photomicrographs of smear slides of sediment-trap samples representing: (**a**, **c**) 'winter' (late September to late June), and (**b**, **d**) 'summer' (late June to late September). In samples accumulated over the 'winter', biogenic silica (diatoms) dominated the inorganic fraction in the upper trap (at the base of the epilimnion, 5.5 m), and relatively few calcite crystals < 5 µm in diameter were observed. Calcite crystals are slightly more abundant and larger in the lower trap (along the chemocline, 15.5 m), but diatoms remain common. Minute crystals of endogenic calcite were abundant in the sample from the upper trap representing 'summer' sedimentation, together with diatoms, and the lower trap contained almost exclusively large calcite crystals. Scale bar = 50 µm

correlated with Fe ($r = -0.71$), Ti ($r = -0.65$) and K ($r = -0.4$). Lead (Pb) and copper (Cu) increased from the 1930s through the 1960s and are inversely correlated with Ca ($r = -0.47$, -0.31 respectively) through the interval above the proposed base of the Anthropocene (1950) (Fig. 8b), and are positively correlated with terrigenous elements Fe, K and Ti elsewhere in the core.

Although analysed at much lower resolution, µ-XRF analysis of subsamples from core CL-19 reveal a marked increase of terrigenous element abundance, including K, during the late nineteenth and mid-twentieth centuries, and during the Indigenous settlement phase (thirteenth to early sixteenth centuries). The peaks in terrigenous elements are attributed to land disturbance, increased soil erosion and runoff in the Crawford Lake catchment. The terrigenous elements abundances closely parallel cultigens and NAP profiles, with a marked decrease between the intervals of Indigenous and colonial settlement, as previously

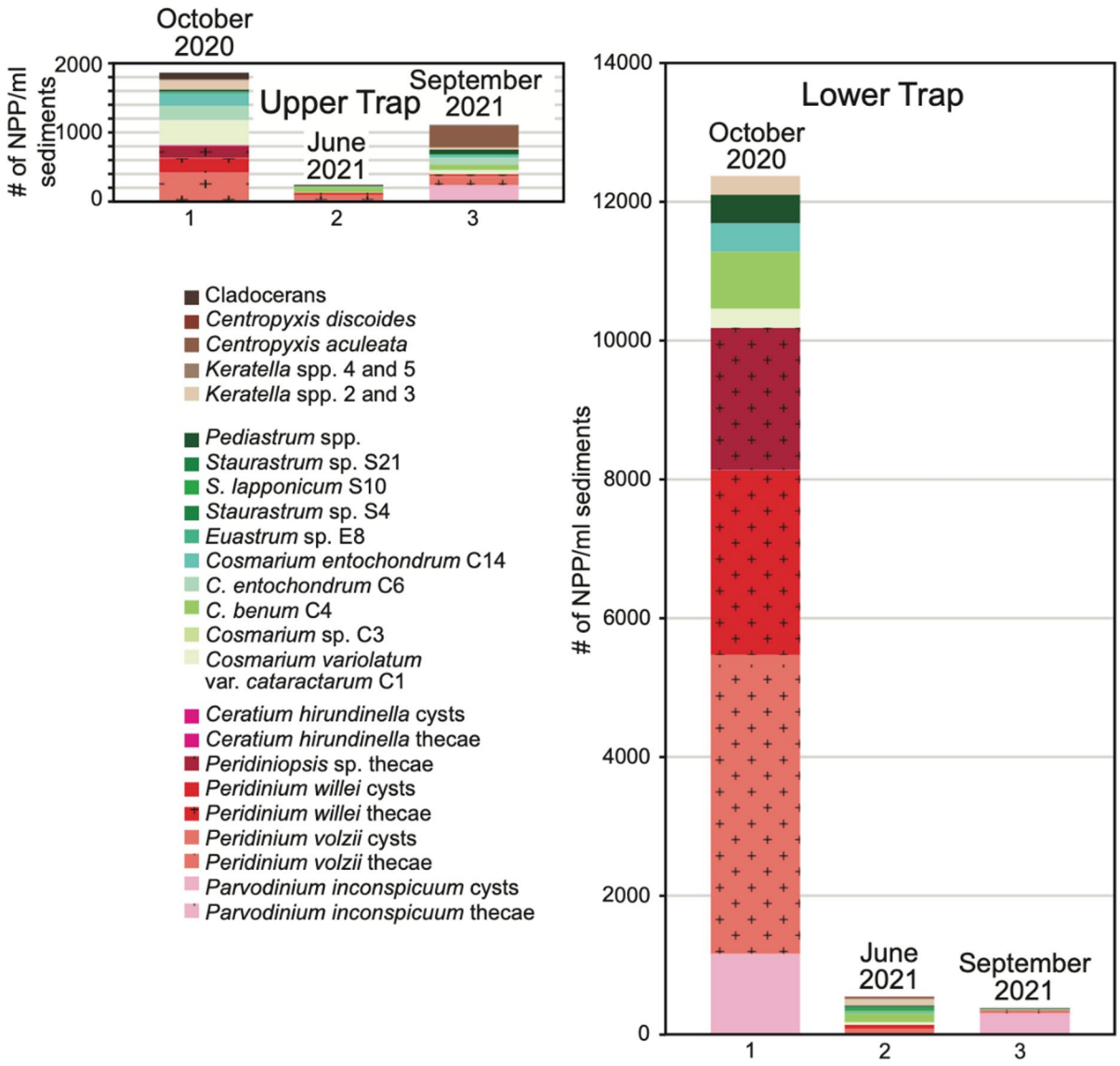

Fig. 7 Influx of organic-walled algae to sediment traps deployed at the base of the epilimnion (upper trap) and along the chemocline (lower trap) in Crawford Lake. Sedimentation intervals represent mid-August to mid-October 2020 ('October'), mid-October 2020 to mid-June 2021 ('June'), and mid-June to mid-September 2021 ('September'). Most of the non-pollen palynomorphs that accumulate on the lakebed (e.g., the > 700,000 algal palynomorphs in the sample collected from the lower trap in October 2020) sink through the isopycnal mixolimnion during fall turnover, representing mass die-off in response to cooling surface waters and declining incident solar radiation

identified by Ekdahl et al. (2007) using standard ICP-MS techniques. Newly acquired radiocarbon ages of seven upland-plant macrofossils also broadly confirm the ages suggested by Ekdahl et al. (2004) for the Indigenous Agricultural Zone at Crawford Lake, but they suggest site abandonment a few decades later, during the early sixteenth century (Table 4).

Applying the transfer functions of Bartlein and Whitlock (1993) to pollen data from core CL-19 identified variations in summer and winter temperature (Fig. S4, Table S6) over the past millennium that compare well with available instrumental data and with published reconstructions (Mann 2002, Mann et al. 2009). Although pollen assemblages have been

Table 3 Influx of organic-walled constituents (individuals per day) to sediment traps at the base of the epilimnion (A) and along the chemocline (B)

A) Upper Trap	Oct-20	Jun-21	Sep-21
Dinoflagellates:			
***Parvodinium inconspicuum* thecae**	**0**	**1.4**	**0**
Parvodinium inconspicuum cysts	19.5	21.6	235.7
***Peridinium volzii* thecae**	**400.4**	**72.1**	**122.6**
Peridinium volzii cysts	0	2.9	9.4
***Peridinium willei* thecae**	**205.1**	**26.0**	**23.6**
Peridinium willei cysts	9.8	8.7	4.7
***Peridiniopsis* sp. Thecae**	**166.0**	**0**	**0**
***Ceratium hirundinella* thecae**	**9.8**	**0**	**0**
***Ceratium hirundinella* cysts**	**9.8**	**0**	**0**
Green algae:			
Cosmarium variolatum	361.4	0	61.3
Cosmarium sp.	0	2.9	0
Cosmarium benum	0	73.6	80.1
Cosmarium entochondrum	380.9	11.5	141.4
Euastrum sp.	19.5	0	0
Staurastrum sp. S4	9.8	0	0
S. lapponicum	0	5.8	9.4
Staurastrum sp. S21	0	0	0
Pediastrum spp.	29.3	0	66.0
Consumers:	136.8	8.7	28.3
Keratella cf. *quadrata*			
Keratella cf. *cochlearis*	0	0	0
Cladoceran	97.7	5.8	9.4
(B) Lower Trap	Oct-20	Jun-21	Sep-21
Dinoflagellates:			
Parvodinium inconspicuum thecae	0	0	0
Parvodinium inconspicuum cysts	1162.1	10.7	301.2
***Peridinium volzii* thecae**	**4170.1**	**0**	**38.7**
Peridinium volzii cysts	136.7	67.0	0
***Peridinium willei* thecae**	**2597.7**	**0**	**11.1**
Peridinium willei cysts	68.4	58.9	0
***Peridiniopsis* sp. Thecae**	**2050.8**	**0**	**0**
***Ceratium hirundinella* thecae**	**0**	**0**	**0**
***Ceratium hirundinella* cysts**	**0**	**0**	**0**
Green algae:			
Cosmarium variolatum	273.4	37.5	0
Cosmarium sp.	0	2.7	0
Cosmarium benum	820.3	128.6	0
Cosmarium entochondrum	410.2	24.1	11.1
Euastrum sp.	0	0	0
Staurastrum sp. S4	0	10.7	0
S. lapponicum	0	34.8	0
Staurastrum sp. S21	0	26.8	2.8

Table 3 (continued)

(B) Lower Trap	Oct-20	Jun-21	Sep-21
Pediastrum spp.	410.2	13.4	5.5
Consumers:			
Keratella cf. *quadrata*	273.4	88.4	11.1
Keratella cf. *cochlearis*	0	8.0	2.8
Cladoceran	273.4	101.8	5.5

Bold, constituents with little/no fossilization potential, and the planktonic herbivores that graze on the phytoplankton (dinoflagellates and green algae)

artificially altered by deforestation since the early nineteenth century, with abundant non-arboreal pollen resulting from land clearing rather than climate change above 25.5 cm (the *Ambrosia* rise), the average temperature reconstructed through the proposed Anthropocene is 21.1 °C for July and −4.3 °C for January, which is very close to instrumental records of modern mean temperatures (around 21 °C and −4 °C, respectively, for weather stations near Crawford Lake; Canadian Climate Normals-Climate-Environment and Climate Change Canada (meteo.gc.ca)). The reconstruction of significantly colder mean January temperatures between the late seventeenth and mid-nineteenth centuries is consistent with the peak of the Little Ice Age (Lamb 1972), largely reflecting the dominance of pine (*Pinus*) pollen, with the only common hardwood pollen being birch (*Betula*) (Fig. S4). This is the culmination of gradual cooling since the Medieval Warm Period (MWP, 74.5–63.5 cm in core CL-19) and is clearly represented by the increase in pine pollen at the expense of thermophilous hardwoods, initially beech (*Fagus*) and maple (*Acer*) and subsequently oak (*Quercus*). Cooling in the late thirteenth century reconstructed by transfer functions may reflect the increase in cultigens and grasses that make up the bulk of the non-arboreal pollen sum, recording establishment of the agricultural settlement together with an increase in fungal pathogens of crops typical of Three Sisters agriculture (Fig. 8). This possibly explains why apparent cooling at Crawford Lake dated to the latest thirteenth century leads the cooling in the circum-North Atlantic region and entire northern hemisphere by several decades (Mann et al. 2009). It is possible that cooler temperatures (notably during winter; Fig. S4) favoured the establishment of fixed settlements with longhouses and abandonment of the agricultural settlement as suggested by the near-disappearance of the pollen of cultigens and spores of their pathogens (Fig. 9). The loss of cultigens and spores have also been noted by other authors (Ekdahl et al. 2004; McAndrews and Turton 2010). This precedes the dramatic Little Ice Age cooling of the mid-seventeenth century recorded at Crawford Lake and throughout the northern hemisphere.

Discussion: the nature of varves

Dark 'winter' laminae are common in non-nutrient-limited temperate lakes when much of the biomass of phytoplankton and their consumers accumulates as organic detritus on the lakebed, with the largest influx of TOC occurring in the fall (Zolitschka et al. 2015). Analysis of the contents of sediment traps at the base of the epilimnion and along the chemocline shows that most of the organic matter reaches the lakebed in the deep basin of Crawford Lake during fall turnover, confirming the observations of Dickman (1979, 1985) (Fig. 6, Table 3). The mass mortality of phytoplankton, in response to shorter days and lower angle of incidence of solar radiation, combined with the breakdown of strong thermal stratification that develops in the mixolimnion through the summer, results in rapid sinking of organic detritus to the lakebed. This is confirmed by the highest concentration of organic-walled plankton in the sample collected from the lower trap (along the chemocline) in mid-August–mid-October, with concentrations more than six times higher than in the second richest sample, collected from the upper trap (at the base of the chemocline) that same day. The high relative abundance of rotifers and cladocerans at the base of the epilimnion during this interval and along the chemocline during mid-October–mid-June (Table 3) supports the hypothesis that

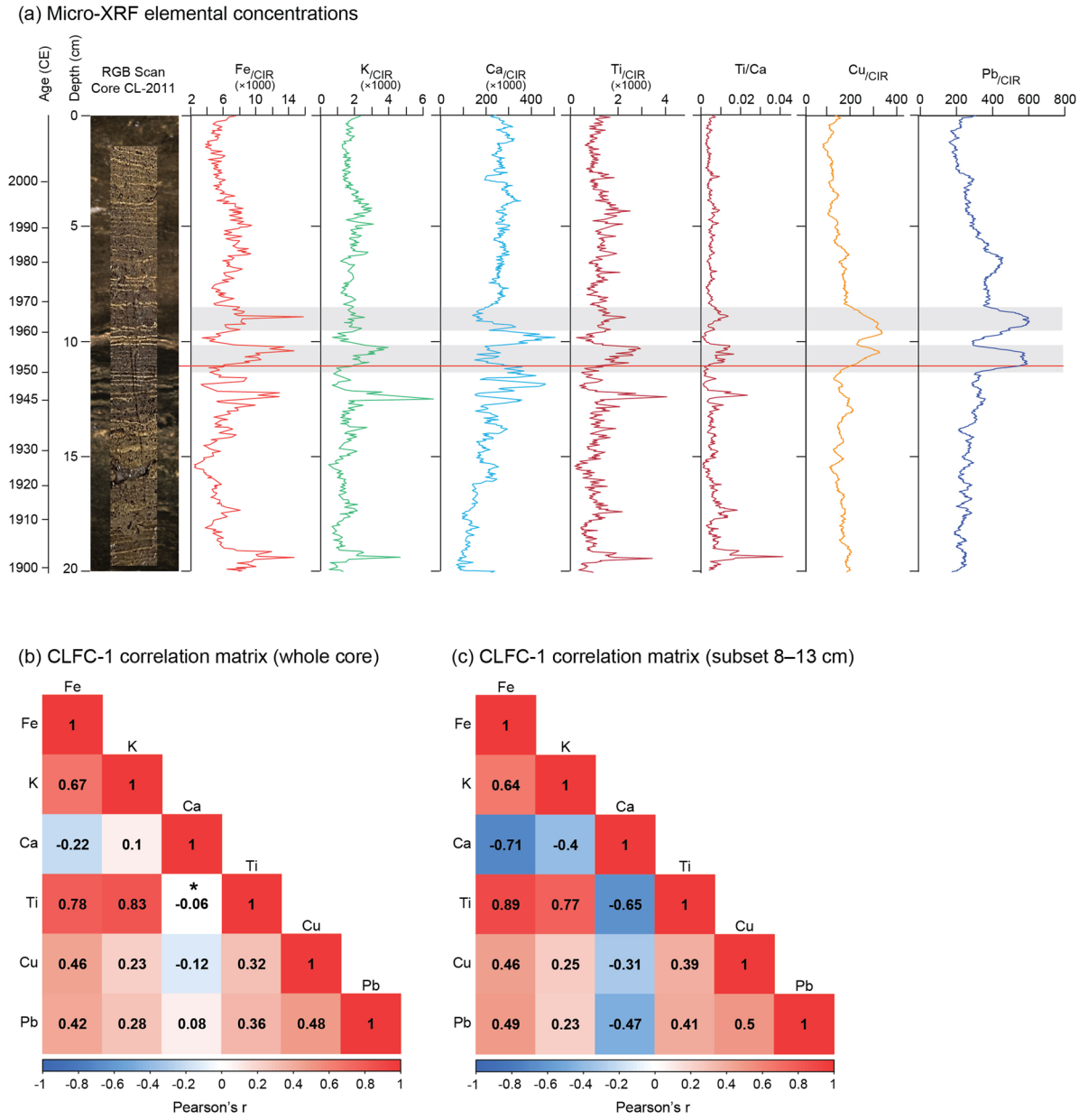

Fig. 8 **a** RGB scan and μ-XRF elemental profiles for freeze core CL-2011 and Pearson correlation matrix for **b** the entire 20 cm freeze-core section and **c** for a section of freeze core (8–13 cm), spanning ~ 1940 through 1975 CE. Red indicates positive correlation and blue inverse correlation, with darkest shades identifying strongest correlation. All but one correlation is significant (* indicates $p < 0.05$). Calcium (Ca) peaks correspond with thick white laminae of authigenic calcite. Ca is an abundant element throughout the freeze core suggesting that calcite is also present in the dark portion of annual varve couplets but in lower abundance. The centimeter-thick dark bands above and below the prominent calcite laminae deposited during the summers of 1956, 1957 and 1958 are evident in the RGB scan, and are associated with increased abundances of terrigenous elements potassium (K), titanium (Ti) and iron (Fe). Anti-correlation of Ca and Ti suggests dissolution of authigenic calcite and enhanced inputs of terrigenous sediments and heavy metals (e.g., copper (Cu), lead (Pb)) from runoff during the 1950s through 1960s, consistent with high influx of fly ash (SCPs in Fig. 3)

Table 4 Radiocarbon ages of plant macrofossils bracketing the Indigenous Agricultural Zone (grey shading identifying palynological samples with evidence of cultigens) in core CL-19, analysed at the A.E. Lalonde AMS Laboratory, University of Ottawa

Lab ID	Submitter ID depth (cm)/ stratigraphic position	^{14}C yr BP	F^{14}C	cal yr BP/mean year CE
UOC-19148 Cedar leaf tip	37–38 cm 2–3 cm above record of Indigenous cultigens	245 ± 14	0.9699 ± 0.0017	310–285 cal (77.2%)/**1653 CE** 167–155 cal (18.3%)
UOC-19149 Cedar leaf tip	38–39 cm 1–2 cm above record of Indigenous cultigens	294 ± 14	0.9641 ± 0.0017	430–372 cal (66.9%)/**1549 CE** 327–301 cal (28.5%)
UOC-19148 deciduous leaf	52–53 cm Between two main peaks in Indigenous cultigens	400 ± 14	0.9514 ± 0.0017	505–455 cal (92.1%)/**1470 CE**
UOC-19148 deciduous leaf	64–65 cm Base of proxy record of Indigenous cultigens	707 ± 15	0.9518 ± 0.0017	676–651 cal (95.4%)/**1287 CE**
UOC-19148 deciduous leaf	78–79 cm 13 cm below record of Indigenous cultigens	1110 ± 15	0.8709 ± 0.0016	1078–1017 cal (42.2%) 1011–959 cal (53.3%)/**942 CE**
UOC-19148 Maple key	83–84 cm 19 cm below record of Indigenous cultigens	1282 ± 15	0.8525 ± 0.0016	1278–1177 cal (95.4%)/ **773 CE**
UOC-19148 deciduous leaf	84–85 cm 20 cm below record of Indigenous cultigens	1327 ± 15	0.8478 ± 0.0016	1295–1261 cal (61.5%)/**672 CE** 1209–1176 cal (33.3%)

Calibration was performed using OxCal v4.3 (Bronk Ramsey 2009) with the calibration curves IntCal13 (Reimer et al. 2013) and Bomb13NH1 (Hua et al. 2013)

Material codes are described in Crann et al. (2017)

microscopic invertebrates migrate to the monimolimnion during fall turnover and over-winter in the relatively warm waters that are rich in dissolved carbon and amorphous and particulate organic matter (Heyde 2021). The thickness of the dark organic layers is thus a function of primary and secondary production in the mixolimnion (greatest in the epilimnion and uppermost metalimnion), which depends on the availability of limiting nutrients, and climate.

The strong radiocarbon-bomb signature measured in particulate and dissolved organic carbon in both the mixolimnion and monimolimnion, as well as in bulk sediments of mid-twentieth century age, supports the dominant authigenic nature of the particulate and amorphous organic matter in this karstic basin (McCarthy et al. 2023). The abundant cellulosic dinoflagellate thecae captured in the water column are rarely preserved, but the organic laminae in Crawford Lake are rich in amorphous organic matter derived from the bacterial decay of these and other labile organic remains, together with pollen and non-pollen palynomorphs comprising various resistant biomolecules (McCarthy et al. 2021). The sediment-trap samples were not examined for prokaryotes, nor from the palynological preparations, since most would be lost through the 15-µm sieve. Fossil pigment data confirm the observation of cyanobacteria in the water column of Crawford Lake, but they have been a minor constituent of the phytoplankton since the mid-nineteenth century (McCarthy et al. 2023) when colonial land clearing began in the Crawford Lake catchment.

The suggestion by Dickman (1979, 1985) that much of the organic matter consists of the remains of anaerobic purple sulfur bacteria has recently been called into question by fossil pigment data and by instrumental measurements of dissolved oxygen that failed to identify anoxia anywhere in the water column of Crawford Lake over a 3-year interval (Heyde 2021; Llew-Williams 2022). Okenone, the pigment characteristic of these obligate anaerobes, is absent from sediments younger than the earliest sixteenth century (Heyde 2021; McCarthy et al. 2023; P. Leavitt unpublished data). The fossil pigment record supports eukaryotic algae as the dominant phytoplankton through the Canadian Zone (since 1867 CE). The common cysts of dinoflagellates (*Parvodinium inconspicuum, Peridinium volzii* and *P. willei*) and the conjugated cells of desmids (mainly *Cosmarium* and *Staurastrum* spp.) were the most common algal palynomorphs identified in palynological preparations of varved sediments from Crawford Lake (Krueger and McCarthy 2016; McCarthy et al. 2018, 2023), as they were in the sediment traps (Fig. 7). The much lower relative abundance of zooplankton in most sediment-trap samples is typical of lacustrine food webs,

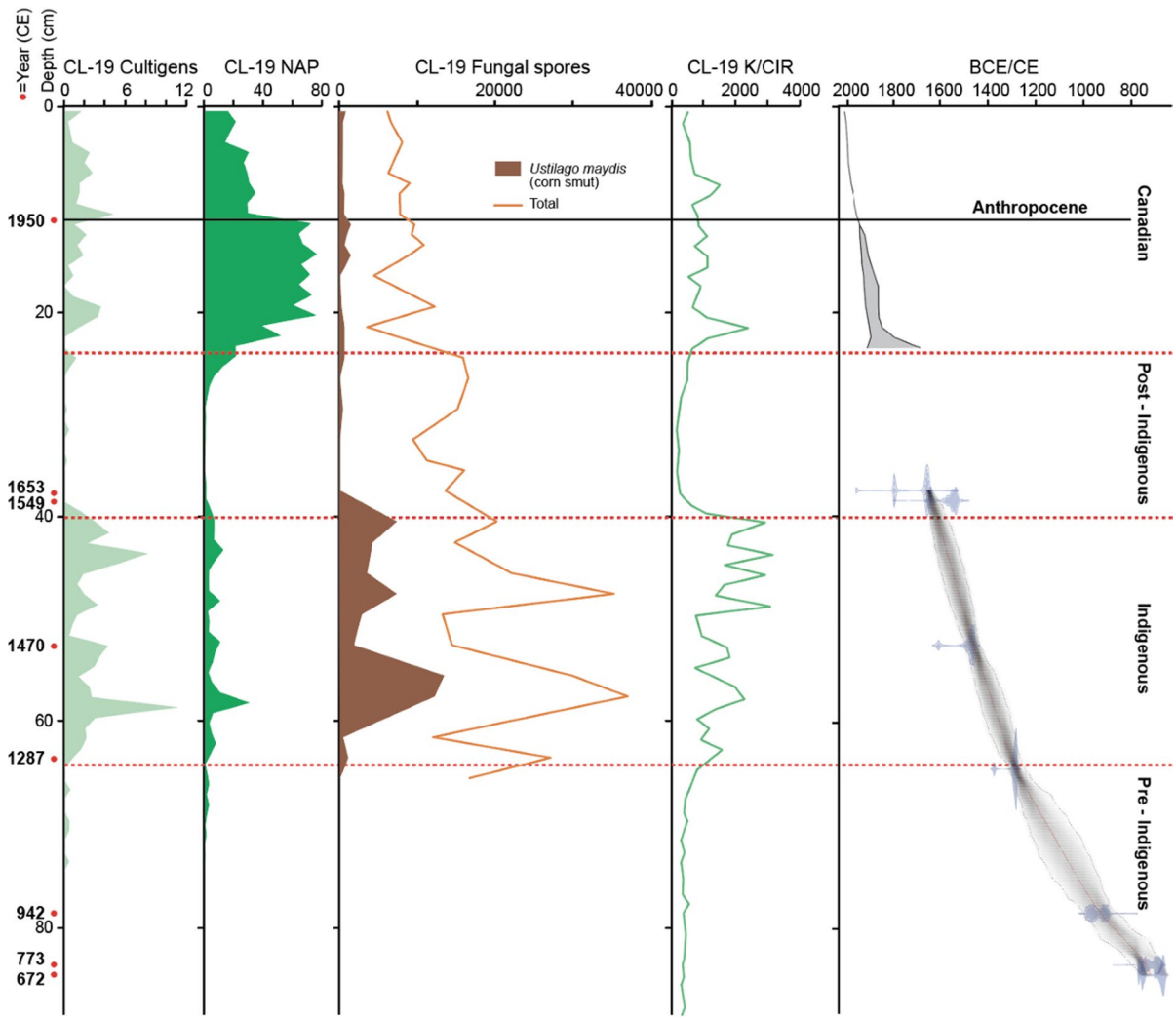

Fig. 9 Core CL-19 cultigens, non-arboreal pollen (NAP), fungal spores (including corn smut/ *Ustilago maydis*) potassium (K) profiles and BACON age model; red dots = absolute ages determined from radiocarbon analysis (Table 4) and the lead-210 age model for the 1950 CE base of the proposed Anthropocene, independently supported by a peak in cesium-137 (McCarthy et al. 2023). Indigenous agricultural activity indicated by rise in cultigens and increase in terrigenous elements (e.g., K) attributed to soil erosion and runoff from the Crawford Lake catchment. The occurrence of two peaks in cultigens in the late thirteenth through fifteenth centuries is largely consistent with the span reported by Ekdahl et al. (2004) except that it suggests abandonment several decades later, during the early sixteenth century

and the exception in the lower trap during fall turnover suggests that microscopic invertebrates survive the winter by feeding on detritus rather than grazing, as suggested by Heyde (2021).

Endogenic calcite is commonly precipitated in hard water lakes during the summer (Brunskill 1969), and this was the mechanism suggested by Dickman (1979, 1985) for the light-coloured laminae in varved sediments from Crawford Lake. LSI calculations suggest that organic sediments are capped by a layer of endogenic calcite ($CaCO_3$) that precipitate when water temperatures in the upper 6 m of Crawford Lake exceed 15 ºC, pH is slightly basic, and concentrations of calcium and carbonate ions are sufficient for supporting calcite formation (Fig. 4a) and are corroborated by SI calculations completed on the same dataset (Table 2). This is consistent with the experimental findings of Coto et al. (2012) who analysed

the solubility of calcite in relation to a multitude of factors including atmospheric carbon dioxide (CO_2) that lowers a solution's pH through carbonic acid (H_2CO_3) dissolution (Eq. 3), and water temperature related to the ability of colder water to hold more dissolved gases in solution (Eq. 3).

$$H_2O + CO_2 \rightleftharpoons H_2CO_3 \rightleftharpoons H^+ + HCO_3^- \rightleftharpoons H_20 + CO_3^{-2} \quad (3)$$

where H_2O—water, CO_2—un-dissociated carbon dioxide gas from atmosphere or in situ biotic respiration, H_2CO_3—carbonic acid, H^+—hydronium ion; HCO_3^-—bicarbonate ion, CO_3^{-2}—carbonate ion.

Photosynthetic carbon fixation removes CO_2 from the water, leading to increasing pH in the epilimnion and upper metalimnion and driving Eq. (4) to the left. With higher pH, precipitation of inorganic calcite crystals will be favoured. These minute crystals sink through the mixolimnion where the pH is lower. As acidity increases, dissolution of calcite crystals is expected. As the calcite approaches higher density waters at the pycnocline, descent will slow which should cause further dissolution of calcite. However, this permanent chemocline contains elevated concentrations of calcium (Ca^{+2}) and alkalinity ($CO_3^{-2} + HCO_3^-$) ions resulting from the influx of bottom waters to the monimolimnion (Fig. 4). This slows calcite dissolution, allowing calcite crystals to complete their descent to the lakebed through the monimolimnion. Elevated calcium and alkalinity concentrations in these bottom waters are associated with groundwater recharge (Apolinarska et al. 2020, 2021) through a dolomitic substrate which is recharged below the chemocline (Priebe et al. 2018; Llew-Williams 2022).

$$CaCO_3 + H_2CO_3 \rightleftharpoons Ca^{+2} + 2HCO_3^- \quad (4)$$

where $CaCO_3$—undissociated calcium carbonate (calcite), H_2CO_3—carbonic acid, Ca^{2+}—'free' calcium ions, HCO_3^-—bicarbonate ions.

Microscopic examination of the inorganic fraction of the sediment traps at the base of the epilimnion confirms that abundant minute crystals of calcite precipitate in the slightly alkaline surface waters during the summer, but they were rare in the sample representing sedimentation between mid-October and mid-June where detrital silicates and biogenic silica were the most abundant particles following treatment with hydrogen peroxide (Fig. S3). Calculations based on physicochemical data collected between August 2018 and September 2021 yielded positive LSI values (corroborated by SI values) only between spring and fall turnover (Figs. 4, 5).

Additionally, LSI calculations suggest conditions for calcite formation were only met within the upper 6 m of the water column, and typically in the upper 2 m, although sometimes not at the surface and presumably due to dilution by in-lake precipitation and surface runoff (Table 2). LSI calculations also suggest that during the cooler months, and deeper in the water column, conditions for calcite formation were not met (Llew-Williams 2022). Photoinhibition of primary production at the surface is a potential contributor to slightly lower pH than observed in the lower epilimnion and upper metalimnion, where high rates of photosynthesis (and hence carbon fixing) are recorded by peak measurements of dissolved oxygen (Heyde 2021). Alternatively, high dissolved oxygen measurements may indicate oxygen trapping along the strong seasonal thermocline that develops in the metalimnion (Wilkinson et al. 2015).

Our measurements demonstrate that although Crawford Lake occupies a dolomitic limestone sinkhole, the conditions producing positive LSI and SI values are marginal. Emissions associated with the dramatic increase in fossil fuel combustion that drove the Great Acceleration of the mid-twentieth century (Syvitski et al. 2020; Head et al. 2022), particularly the coking coal at Hamilton steel mills located 30 km upwind (McCarthy et al. 2023) appears to have lowered the pH of the epilimnion sufficiently to make most summers from the mid-1940s through early 1970s difficult to discriminate in dark-coloured parts of the varved succession where calcite laminae are very thin (Fig. 2). Siliceous microfossil assemblages in varved sediments with very thin calcite laminae (Fig. 3) record increased light penetration during the summer (Gushulak et al. 2022; Marshall et al. 2023) and this could have resulted from a reduction in precipitation of calcite crystals in the upper mixolimnion. Peak concentrations of SCPs (spheroidal carbonaceous particles/fly ash) and depleted $\delta^{15}N$ values record increased fossil fuel combustion (Fig. S1), corroborating the hypothesis that acid rain leached terrigenous elements from soils in the catchment and metals common in SCPs and concentrated these in centimeter-thick layers above and below a distinctive

triplet of prominent calcite laminae assigned to the summers of 1956, 1957, and 1958 (Fig. 8). µ-XRF analysis performed on the CL-2011 core records an influx of terrigenous sediments to the lake basin relative to $CaCO_3$ production under increased anthropogenic industrialization (Fig. 8). The increasing impacts of atmospheric pollution resulting from rapid industrialization and urbanization of southern Ontario are also indicated by an increase in lead and copper from the 1930s through the 1960s, attributed to increased atmospheric influx of SCPs during the Great Acceleration (Steffen et al. 2015) prior to controls on emissions from blast furnaces in Hamilton (McCarthy et al. 2023). Inorganic ash spheres in fly ash are especially rich in these heavy metals as well as iron (Lan and Breslin 1999).

Ekdahl et al. (2004) reported a discrepancy of more than a century between radiocarbon ages obtained from upland-plant material below the Canadian Zone and counts of calcite laminae to the top of the Indigenous Agricultural Zone that they estimated spanned 1268–1486 CE. Prominent calcite laminae and relatively thick organic laminae containing abundant pollen of cultigens appeared to be deposited annually for 218 years around the middle of the last millennium. Recently obtained radiocarbon ages help bracket the interval of Indigenous agricultural settlement from the late thirteenth to earliest sixteenth centuries (Fig. 9, Table 5), which is more consistent with archeological findings (including radiocarbon ages of charred maize kernels from excavated hearths) that suggest two major intervals of longhouse occupation with a several-decade hiatus during the late fourteenth century (Finlayson 1998; pers. comm.). Lafond et al. (2023) confirmed a disruption of the varve chronology between periods of human impact on the catchment, with ages based on counting white laminae using ultra high-resolution imagery approximately two hundred years younger, as noted earlier by Ekdahl et al. (2004). This is predictable given the cold temperatures reconstructed through the latter part of the Little Ice Age (mid-seventeenth through mid-nineteenth centuries), but the importance of primary production and carbon fixation for varve formation is clear by comparing the typically thick varves with prominent calcite laminae during the Indigenous Agricultural and Canadian zones with the very low sedimentation rates and rare calcite laminae between these intervals of cultural eutrophication. The sediments are not bioturbated, as benthos tolerant of the relatively high salinities have not been able to colonize the deep basin of Crawford Lake. The largest invertebrates are stygofaunal ostracods that entered the monimolimnion via aquifers, but they are not burrowers (Heyde 2021; C. Chan unpublished data). The combination of increased influx of limiting nutrients after land was first cleared for agriculture and the warm temperatures of the Medieval Climate Optimum produced the most prominent calcite laminae of the past millennium during the latest thirteenth through fourteenth centuries (Fig. 2).

Although calcite laminae are present below the *Ambrosia* rise that characterises the Canadian Zone (Fig. 2), conditions required for precipitation of sufficient calcite to form perceptible laminae were not met during the summers of the Little Ice Age (mid-sixteenth to nineteenth centuries; Lamb 1972). Around Crawford Lake, this was marked by increasing abundance of pine at the expense of thermophilous hardwood trees (McAndrews and Turton 2010; McCarthy et al. 2023), evident in reconstructions of much colder than modern temperatures from the seventeenth through mid-nineteenth centuries (Fig. S3). The breakdown of the varve chronology below the Canadian Zone appears to be consistent with the identification of periodicities in varve thickness that correspond with those of major climate cycles using wavelet analysis (Fig. S4).

Conditions producing positive LSI values were also never met below the uppermost mixolimnion despite the very high concentrations of Ca^{+2}, CO_3^{-2} and HCO_3^- in the monimolimnion, due to the consistently low temperatures and slightly acidic conditions. Lower pH is attributed to the very high concentration of dissolved organic carbon from humic acids in the catchment and respiration and decomposition below the chemocline (Llew-Williams 2022).

There is an interesting anomaly between very high measurements of alkalinity and electrical conductivity (reflecting high concentrations of Ca^{+2}, CO_3^{-2} and HCO_3^-) and measurements of pH below 7 in the monimolimnion. The slightly acidic and cold conditions in the dense monimolimnion would dissolve calcite crystals, but high concentrations of ions measured by titration (Table 2, Fig. S2) promote crystallization. Wittkop (2004) also concluded that the monimolimnion of Crawford Lake had a strong buffering capacity that inhibited calcite dissolution.

The physical and chemical contrast along the chemocline appears to allow calcite crystals to grow by accretion and then sink relatively quickly through the slightly acidic waters to the lakebed. Our observations of constituents in the lower sediment trap support this hypothesis, since calcite crystals were larger than in the upper trap. Slightly larger crystals were collected in June, but many times larger than those in the other sediment-trap samples, some exceeding 50 µm in contrast to those in the upper traps that were only a few micrometers in diameter (Fig. 6). This suggests that minute calcite crystals precipitating in the epilimnion and uppermost metalimnion act as nuclei for large crystals when they encounter the calcium and alkalinity concentrations that support calcite formation along the chemocline, where the increase in density slows their descent. When they grow large enough to overcome viscosity (Stokes' Law), they sink relatively quickly through the monimolimnion to the lakebed. Smear slides of the light-coloured laminae comprised calcite crystals almost exclusively smaller than those retrieved from the lower sediment trap (Fig. S5), although siliceous algae were abundant in sediment traps between spring and fall turnover and in sediment samples processed for siliceous microfossil analysis (Gushulak et al. 2022; Marshall et al. 2023). This implies that they are also growing during settling, and subsequently subject to some dissolution during the final phase of settling, as they sink through the slightly acidic monimolimnion.

Conclusions

Combining physical and chemical water properties collected from a permanently stratified varve-forming environment over a multi-year period (Llew-Williams 2022), with detailed sediment trap and sediment-core analysis, provides novel insights into the dynamics influencing the recent sediment records of Crawford Lake and surrounding catchment, as well as the mechanisms and conditions required to support varve formation. The site's well-preserved and documented cultural history makes it an excellent location to study the importance of eutrophication in producing the hydrological conditions conducive to calcite accumulation in the slightly acidic monimolimnion of this unique meromictic lake.

Observational evidence during 50 years of coring supports the contention that varves accumulate below the chemocline, and at no time in the Canadian Zone was calcite accumulation too low to prevent the 'summer' laminae from being discerned in freeze cores from Crawford Lake. This allows (sub)annual chronological precision over the last two centuries (Ekdahl et al. 2004) including across the proposed base of the Anthropocene epoch in the mid-twentieth century (McCarthy et al. 2023).

Ours is the first study to examine the calcite crystals of Crawford Lake and assess the limnological conditions that allow endogenic calcite to precipitate in the alkaline surface waters. Applying LSI calculations to the physical and chemical characteristics of the water column between 2019 and 2021 shows that conditions favourable for calcite precipitation in Crawford Lake are dependent on water chemistry (i.e., calcium ion concentrations and alkalinity), pH values (> 7.8), primary productivity in the epilimnion and uppermost metalimnion (i.e., sequestering of CO_2), and water temperatures (> 15 °C). This explains the diminishment of varve expression between phases of human impact on Crawford Lake during the Little Ice Age, although prominent calcite laminae in sediments rich in the pollen of cultigens and their pathogens and high concentrations of phytoplankton and their consumers link varve formation to human habitation between the late thirteenth and latest fifteenth or earliest sixteenth centuries.

Analysis of material collected in sediment traps over one full hydrologic year confirmed the sedimentation of abundant endogenic calcite in the deep basin of Crawford Lake only between spring and fall turnover. It also presented an unexpected observation: minute calcite crystals precipitated in the upper 6 m of the water column act as nuclei. Where their descent is slowed by the density contrast along the chemocline, they encounter high concentrations of ions and crystal growth continues. These now-larger crystals sink relatively quickly through the slightly acidic monimolimnion to the lakebed, where they are rapidly covered by dominantly authigenic organic matter during fall turnover.

Although the water in the karstic basin of Crawford Lake is well-buffered, even slightly lower pH values in surface waters during the mid-twentieth century were sufficient to reduce the temporal and spatial window conducive to precipitation of endogenic calcite.

Sediments with very thin calcite laminae from the late 1940s through the early 1970s record increased fossil fuel combustion and increased concentrations of terrigenous elements leached from the catchment by acid rain. McCarthy et al. (2023) proposed that the Anthropocene GSSP be placed in core CRA22-1FR-3 at the base of a thin light-coloured lamina deposited in the summer of 1950 CE. This is near the base of the lower of two centimeter-thick dark bands with barely perceptible light-coloured laminae that can easily be correlated across the deep basin of Crawford Lake (e.g., freeze core CRA23-BC-1F-A in Fig. 2), as can the prominent calcite laminae deposited in the summers of 1956, 1957, and 1958 that are readily identifiable in all freeze cores collected (McCarthy et al. 2023). A prominent light-coloured lamina representing the summer of 1948 CE provides another conspicuous marker. Thicker calcite laminae and easily discriminated varves have been deposited since the mid-1970s when more stringent air-quality controls were introduced. Given the rising temperatures and ongoing mesotrophic conditions in Crawford Lake, pronounced varve deposition and hence an annually resolvable sediment record should continue for the foreseeable future.

Acknowledgements A. Alderson, A. Heyde and P.M. Pilkington (Brock University), B. O'Reilly (Conservation Halton), and J.H. McAndrews and S. Finkelstein (University of Toronto) provided field assistance and M. Lozon (Brock University) assisted with drafting. We acknowledge financial support from the Natural Sciences and Engineering Research Council of Canada (F.M., R.T.P., M.J.H., M.P., K.T. and J.B.) and Haus der Kulturen der Welt (F.M.), from Brock University for subsidizing the MSc research of B.L.-W. and postdoctoral appointment of N.R., and from N. Ghazi (E3 Laboratories) for subsidizing analytical costs. Logistical support and permission to perform these analyses and in-kind support from Conservation Halton is gratefully acknowledged. Crawford Lake is located on the traditional territory of the Attawandaron, Wendat, Haudenosaunee and Anishinaabe peoples. We gratefully acknowledge the input of reviewers, notably Dr. Chad Wittkop (Minnesota State University), whose suggestions improved the manuscript.

Author contribution BL-W and FM wrote the main manuscript text, BL-W performed all hydrological analysis under the supervision of FM and with guidance from KT, UB, MJH and MM. AK assisted with sediment trap analysis and sediment core analysis was performed by NR, JB, and KL. RTP, NN, MP and MM assisted with field sampling and radiocarbon analysis. All figures were prepared by BL-W with assistance from FM, MJH and draftsman ML other than Figs. 2 and S4 by KL, and Figs. 8 and 9 by NR, JB and NN. All authors reviewed the manuscript.

Funding The research was funded by NSERC Discovery grants to F. McCarthy, R.T. Patterson, M.J. Head, M. Pisaric, K. Turner and J. Boyce. We acknowledge the Haus der Kulturen der Welt (HKW), Berlin for collaborating with the Anthropocene Working Group in the assessment of the candidate GSSP-sites, which led to this associated project and made use of data from several cores collected as part of that evaluation. Several other institutions have provided in-kind or financial support, including Conservation Halton, Brock University, Carleton University, the Canadian Museum of Nature and the Royal Ontario Museum.

Declarations

Conflict of interest This research was conducted as part of a proposal to the Anthropocene Working Group (AWG) that Crawford Lake be nominated as the Global boundary Stratotype Section and Point (GSSP). Details of these activities are available in Waters et al. (2023).

References

Anderson RY, Dean WE (1988) Lacustrine varve formation through time. Palaeogeog Palaeoclimatol Palaeoecol 62:215–235

Apolinarska K, Pleskot K, Pełechata A, Migdałek M, Siepak M, Pełechaty M (2020) The recent deposition of laminated sediments in highly eutrophic Lake Kierskie, western Poland: 1 year pilot study of limnological monitoring and sediment traps. J Paleolimnol 63:283–304

Apolinarska K, Pleskot K, Pełechata A, Migdałek M, Pełechaty M (2021) Seasonal deposition of authigenic calcite out of isotopic equilibrium with DIC and water, and implications for paleolimnological studies. J Paleolimnol 66:41–53

Armstrong DK, Carter TR (2010) The subsurface Paleozoic stratigraphy of southern Ontario. Ontario Geological Survey, Special Vol 7, 301pp

Bartlein PJ, Whitlock C (1993) Paleoclimatic interpretation of the Elk Lake pollen record. In: Bradbury JP, Dean WE (eds) Elk Lake, Minnesota: evidence for Rapid Climate Change in the North-Central United States. Geol Soc America Spec Pap 276:275–293

Boyko M (1973) European impact of the vegetation around Crawford Lake in Southern Ontario. M.Sc. Thesis, University of Toronto, 110 pp

Boyko-Diakonow M (1979) The laminated sediments of Crawford Lake, southern Ontario, Canada. In: Schluchter C (ed) Moraines and Varves. A. A. Balkema, Rotterdam, pp 303–307

Brunskill GJ (1969) Fayetteville Green Lake, New York. II. Precipitation and sedimentation of calcite in a meromictic lake with laminated sediments. Limnol Oceanogr 14:830–847

Brunton FR (2009) Update of revisions to the early Silurian stratigraphy of the Niagara Escarpment: integration of sequence stratigraphy, sedimentology and hydrogeology to delineate hydrogeologic units. In: Summary of field work and other activities 2009. Ontario Geological Survey Open File Report, vol 6240, pp 25-1–25-20

Coto B, Martos C, Pena JL, Rodriguez R, Pastor G (2012) Effects in the solubility of $CaCO_3$: experimental study and model description. Fluid Phase Equilib 324:1–7

Dickman MD (1979) A possible varving mechanism for meromictic lakes. Quat Res 11:113–124

Dickman MD (1985) Seasonal succession and microlamina formation in a meromictic lake displaying varved sediments. Sedimentology 32:109–118

Ekdahl EJ, Teranes JL, Guilderson TP, Turton CL, McAndrews JH, Wittkop CW, Stoermer EF (2004) A prehistorical record of cultural eutrophication from Crawford Lake, Canada. Geology 32:745–748

Ekdahl EJ, Teranes JL, Wittkop CW, Stoermer EF, Reavie ED, Smol JP (2007) Diatom assemblage response to Iroquoian and Euro-Canadian eutrophication of Crawford Lake, Ontario, Canada. J Paleolimnol 37:233–246

Finlayson W (1998) Iroquoian peoples of the land of rocks and water A.D. 1000–1650: a study in settlement archaeology, vol 1. London Museum Special Publication, London, p 448

Gregory BR, Reinhardt EG, Macumber AL, Nasser NA, Patterson RT, Kovacs SE, Galloway JM (2017) Sequential sample reservoirs for ITRAX-XRF analysis of discrete samples. J Paleolimnol 57:287–293

Gushulak AC, Marshall M, Cumming BF, Llew-Williams B, Patterson RT, McCarthy FMG (2022) Siliceous algae response to the 'Great Acceleration' of the mid-twentieth century in Crawford Lake (Ontario, Canada): a potential candidate for the Anthropocene GSSP. Anthropocene Rev 9(3):571–590

Head MJ, Steffen W, Fagerlind D, Waters CN, Poirier C, Syvitski J, Zalasiewicz JA, Barnosky AD, Cearreta A, Jeandel C, Leinfelder R, McNeill JR, Rose NL, Summerhayes C, Wagreich M, Zinke J (2022) The Great Acceleration is real and provides a quantitative basis for the proposed Anthropocene Series/Epoch. Episodes 45:359–376. https://doi.org/10.18814/epiiugs/2021/021031

Heyde A (2021) Crawford lake consumers: water column and palynological studies. MSc Thesis, Department of Biological Sciences, Brock University

Horiba (2009) Multi Water Quality Checker U-50 Series Instruction Manual. https://www.instrumart.com/assets/Horiba-U50-Manual.pdf

Krueger AM, McCarthy FMG (2016) Great Canadian Lagerstätten 5: Crawford Lake—a Holocene lacustrine Konservat-Lagerstätte with two-century-old viable dinoflagellate cysts. Geosci Can 43:123–132

Lafond KM, Walsh CR, Patterson RT, McCarthy FMG, Llew-Williams BM, Hamilton PB, Nasser NA, Cumming B (2023) Influence of climatic trends and cycles on the annual varve deposition in Crawford Lake, Ontario, Canada. Geosciences 13:87. https://doi.org/10.3390/geosciences13030087

Lamb HH (1972) The cold Little Ice Age climate of about 1550 to 1800. Climate: present, past and future. Methuen, London, p 107

Langelier WF (1936) The analytical control of anti-corrosion water treatment. J Americ Water Works Assoc 28:1500

Langelier WF (1946) Chemical equilibria in water treatment. J Americ Water Works Assoc 38:35

Lan Y, Breslin VT (1999) Sedimentary records of spheroidal carbonaceous particles from fossil-fuel combustion in western Lake Ontario. J Great Lakes Res 25:443–454

Last WM (2001) Mineralogical analysis of lake sediments. In: Last WM, Smol J (eds) Tracking environmental change using Lake sediments, physical and geochemical methods (vol 1). Kluwer, Dordrecht, pp 143–187

Llew-Williams BM (2022) The hydrological and limnological characterization of two Canadian water catchments sensitive to anthropogenic influences: Crawford Lake, Ontario and Old Crow Flats, Yukon, MSc Thesis, Brock University

Mann ME, Rutherford S, Bradley RS, Hughes MK, Shindell D, Ammann C, Faluvegiand G, Ni F (2009) Global signatures and dynamical origins of the Little Ice Age and Medieval Climate Anomaly. Science 326(5957):1256–1260

Mann ME (2002) Medieval climatic optimum volume 1, the earth system: physical and chemical dimensions of global environmental change. In: MacCracken MC, Perry JS (eds), Encyclopedia of global environmental change, pp 514–516. ISBN 0-471-97796-9. Editor-in-Chief Ted Munn. Wiley, Chichester

Marshall MG, Hamilton PB, Lafond KM, Nasser NA, McCarthy FMG, Patterson RT (2023) Annual-scale assessment of mid-twentieth century anthropogenic impacts on the algal ecology of Crawford Lake, Ontario, Canada. PeerJ 11:e14847

McAndrews JH, Turton CL (2010) Fungal spores record Iroquoian and Canadian agriculture in 2nd millennium AD sediment of Crawford Lake, Ontario, Canada. Veg Hist Archaeobot 19:495–501

McCarthy FMG, Riddick NL, Volik O, Danesh DC, Krueger AM (2018) Algal palynomorphs as proxies of human impact on freshwater resources in the Great Lakes region. Anthropocene 21:16–31

McCarthy FMG, Pilkington PM, Volik O, Heyde A, Cocker SL (2021) Non-pollen palynomorphs in freshwater sediments and their paleolimnological potential. In: Marret F, O'Keefe J, Osterloff O, Pound M, Shumilovskikh L (eds) TMS special publication sp511, applications of non-pollen palynomorphs from palaeoenvironmental reconstructions to biostratigraphy. Geological Society of London, London. https://doi.org/10.1144/SP511-2020-109

McCarthy FMG, Patterson RT, Head MJ, Riddick NL, Cumming BF, Hamilton PB, Pisaric MFJ, Gushulak AC, Leavitt PR, Lafond KM, Llew-Williams B, Marshall M, Heyde A, Pilkington PM, Moraal J, Boyce JI, Nasser NA, Walsh C, Garvie M, Roberts S, Rose NL, Cundy AB, Gaca P, Milton JA, Hajdas I, Crann CA, Boom A, Finkelstein SA, McAndrews JH, other members of Team Crawford (2023) The varved succession of Crawford Lake, Milton, Ontario, Canada as a candidate Global boundary Stratotype Section

and Point for the Anthropocene series. Anthropocene Rev. https://doi.org/10.1177/20530196221149281
Morse JW, Arvidson RS, Lüttge A (2007) Calcium carbonate formation and dissolution. Chem Revue 107:342–381
Müller B, Meyer JS, Gächter R (2016) Alkalinity regulation in calcium carbonate-buffered lakes. Limnol Oceanogr 61:341–352
Priebe EH, Brunton FR, Rudolph DL, Neville CJ (2018) Geologic controls on hydraulic conductivity in a karst-influenced carbonate bedrock groundwater system in southern Ontario, Canada. Hydrogeol J 27:1291–1308
Priebe EH (2019) Investigating new approaches for mapping groundwater systems in karstic carbonate bedrock: a case study in the Early Silurian formations of the Niagara Escarpment cuesta, southern Ontario, Canada. PhD Thesis, University of Waterloo
Randsalu-Wendrup L, Conley DJ, Carstensen J (2014) Combining limnology and palaeolimnology to investigate recent regime shifts in a shallow, eutrophic lake. J Paleolimnol 51:437–448
Riddick NL, Volik O, McCarthy FMG, Danesh DC (2017) The effect of acetolysis on desmids. Palynology 41:171–179
Rothwell R, Croudace I (2015) Micro-XRF studies of sediment cores: a perspective on capability and application in the environmental sciences. In: Croudace I, Rothwell R (eds) Micro-XRF studies of sediment cores. Developments in Paleoenvironmental Research (vol 17). Springer, Dordrecht
Rybak M, Dickman M (1988) Paleoecological reconstruction of changes in the productivity of a small, meromictic lake in Southern Ontario, Canada. Hydrobiologia 169:293–306
Steffen W, Broadgate W, Deutsch L, Gaffney O, Ludwig C (2015) The trajectory of the Anthropocene: the great acceleration. Anthropocene Rev 2:81–98
Steffen W et al (2016) Stratigraphic and earth system approaches to defining the Anthropocene. Earth's Future 4:324–345
Syvitski J, Waters CN, Day J, Milliman JD, Summerhayes C, Steffen W, Zalasiewicz J, Cearreta A, Gałuszka A, Hajdas I, Head MJ, Leinfelder R, McNeill JR, Poirier C, Rose NL, Shotyk W, Wagreich M, Williams M (2020) Extraordinary human energy consumption and resultant geological impacts beginning around 1950 CE initiated the proposed Anthropocene Epoch. Commun Earth Environ 1:32. https://doi.org/10.1038/s43247-020-00029-y
Waters CN, Turner SD, Zalasiewicz J, Head MJ (2023) Candidate sites and other reference sections for the Global boundary Stratotype Section and Point (GSSP) of the Anthropocene series. Anthropocene Rev 10:3–24
Wilkinson GM, Cole JJ, Pace ML, Johnson RA, Kleinhans MJ (2015) Physical and biological contributions to metalimnetic oxygen maxima in lakes. Limnol Oceanogr 60:242–251
Wittkop CA (2004) Paleoenvironmental reconstruction using laminated sediments containing authigenic carbonate minerals: case studies from the Great Lakes region of North America. Dissertation, University of Minnesota, 201 pp
Zalasiewicz J, Waters CN, Williams M, Summerhayes C (eds) (2019) The anthropocene as a geological time unit: a guide to the scientific evidence and current debate, 361 pp. Cambridge, UK: Cambridge University Press
Zolitschka B, Francus P, Ojala AEK, Schimmelmann A (2015) Varves in lake sediments—a review. Quat Sci Rev 117:1–41

Publisher's Note Springer Nature remains neutral with regard to jurisdictional claims in published maps and institutional affiliations.

Springer Nature or its licensor (e.g. a society or other partner) holds exclusive rights to this article under a publishing agreement with the author(s) or other rightsholder(s); author self-archiving of the accepted manuscript version of this article is solely governed by the terms of such publishing agreement and applicable law.